# Lithostratigraphic and structural reconstruction of the Zn-Pb-Cu-Ag-Au Lemarchant volcanogenic massive sulphide (VMS) deposit, Tally Pond group, central Newfoundland, Canada

Jonathan Cloutier[1*,**], Stephen J. Piercey[1], Stefanie Lode[1], Michael Vande Guchte[2] and David A. Copeland[2]

[1] Department of Earth Sciences, Memorial University of Newfoundland, 300 Prince Philip Drive, St. John's, Newfoundland and Labrador, Canada, A1B 3X5.

[2] Canadian Zinc Corporation, Suite 1710, 650 West Georgia Street, PO Box 11644, Vancouver, British Columbia, Canada, V6B 4N9

- [*]Corresponding author: jc301@st-andrews.ac.uk
  - Phone: +44 (0) 1334 464948
- [**] Current address - Department of Earth and Environmental Sciences, University of St Andrews, North Street, St Andrews KY16 9AL, UK

## Abstract

The Lemarchant volcanogenic massive sulphide (VMS) deposit (1.24 Mt grading at 0.58% Cu, 5.38% Zn, 1.19% Pb, 1.01 g/t Au, and 59.17 g/t Ag) is a bimodal-felsic VMS deposit hosted within the Late Cambrian (~513-509 Ma) Tally Pond group of the Exploit Subzone in central Newfoundland, Canada. The deposit is hosted by andesitic volcaniclastic and volcanic rocks with subordinate dacite flows. The mineralisation is hosted by the dacites and is overlain by pillowed and massive basalts.

Four structural breaks offset the local stratigraphic sequences including: 1) the LJ syn-volcanic shear zone; 2) the KJ syn-volcanic shear zone; 3) the Lemarchant thrust; and 4) the Bam normal fault. Deformation of the Lemarchant likely occurred during the Penobscot orogeny (486-478 Ma). Early deformation is marked with the local deformation of the LJ and KJ syn-volcanic shear zones during NW-SE compression which coincided with the development of the Lemarchant thrust. A late (< 465 Ma) east trending normal fault, the Bam fault, affected the central portion of the Lemarchant area and down-faulted the southern portion of the study area relative to the northern portion.

Immobile element systematics of all the sequences from the Lemarchant deposit are tholeiitic with transitional Zr/Y ratios (1.9–6.6), $La_n/Sm_n$ ratios <1 (normalised to upper crust), and have primitive mantle extended rare earth elements profiles with slight light rare earth element (LREE)-enriched patterns with flat heavy REE (HREE), and weak to strong negative Nb, Zr, and Ti anomalies. Together, these geochemical features, coupled with an FIIIa signature, and existing mineralogical and Nd-Pb isotope data, are consistent with the rocks at the Lemarchant deposit having formed within a shallow (<1500m) arc or migrating cross-arc seamount chain located within a young peri-

continental rifted arc along the margin of Ganderia, within the Iapetus Ocean. The estimated shallow water emplacement of the deposit likely allowed boiling near or at the rock-sea water interface, ultimately resulting in precious metal enrichment of the Lemarchant deposit. It is suggested that cross-arcs within rifted arc environments may represent favourable exploration targets for precious metal-enriched VMS deposits.

**Keywords:** precious metal enriched VMS deposits; Lemarchant deposit; Tally Pond; stratigraphic reconstruction; structural reconstruction; Appalachian tectonic evolution.

## 1. Introduction

The Lemarchant deposit is a type example of an Appalachian precious metal-bearing bimodal-felsic volcanogenic massive sulphide (VMS) deposit (Fig. 1). Globally, bimodal-felsic (i.e., Kuroko-type) VMS deposits are commonly Zn-Pb-Cu-rich, stratabound to stratiform, syngenetic deposits that form on, or near, the seafloor by precipitation from hydrothermal fluids (e.g., Large, 1977; Franklin et al., 1981, 2005; Lydon, 1984, 1988; Hannington, 2014). They are commonly capped by massive barite and hydrothermal exhalative mudstone.

Bimodal-felsic hosted deposits form near eruptive centres and are commonly hosted within autoclastic rhyolitic volcaniclastic rocks to massive rhyolite flows (e.g., Ohmoto 1996; Lizasa et al. 1999; McNicoll et al. 2010; Piercey et al. 2014). Bimodal-felsic deposits, like all VMS deposits, form within extensional geodynamic regimes, commonly in arc rifts and back-arc basins (e.g., Swinden 1991; Piercey 2010, 2011; Hannington 2014). In ancient environments, the extensional stage of tectonic activity is frequently followed by uplift, basin inversion, compressional deformation, and metamorphism of the sequence hosting the massive sulphide deposits often related to post-VMS formation accretionary tectonics (e.g., McClay 1995; Nelson 1997). Consequently, lithostratigraphic and structural reconstructions of VMS deposits in ancient accretionary orogens are critical to understand the genesis of ancient VMS deposits, as well as their exploration.

The Lemarchant deposit provides the opportunity to study deformed VMS mineralisation systems in an accretionary orogenic setting. The level of stratigraphic preservation and the predominantly brittle deformation at Lemarchant allows for its

reconstruction in 3D, unlike many other volcanic belts where high intensity of deformation obscures original stratigraphy (i.e., more structurally complex and ductile in nature) or where outcrop distribution and diamond drilling density are insufficient to undertake the reconstruction. The aim of this study is to document the stratigraphy and major structures affecting the Lemarchant VMS deposit to understand the subsurface distribution of the structural features and geologic units, including the mineralisation, using a three-dimensional framework. In addition, this study presents new geochemical data obtained at the Lemarchant deposit and assess the immobile element geochemical signatures and the tectonic evolution of the Lemarchant deposit and Tally Pond group. This reconstruction resolves the primary origin for mineralised zones, provides new information on the tectonic evolution of the Tally Pond group and the Appalachian mountain belt, and generates new exploration concepts for VMS deposits. The results herein have implications not only for Appalachian VMS environments, but for any deformed and imbricated VMS belts globally.

## 2. Geology

### *2.1 Regional Geology*

The Cambrian (513-509 Ma) Lemarchant VMS deposit is located within the Dunnage Zone of the Appalachian mountain belt of central Newfoundland, Canada (Fig.1; Copeland 2008). The Dunnage Zone is bounded by the Humber Zone to the west and the Gander Zone to the east (Williams 1979; Williams et al. 1988; Hibbard et al. 2004), and represents the deformed vestiges of arcs, back-arcs and ophiolite complexes assembled during the closure of the Cambrian to Ordovician Iapetus Ocean (Fig. 1;

96 Williams 1979; Williams et al. 1988; Swinden et al. 1989; Swinden 1991; Kean et al.
97 1995; van Staal and Colman-Sadd 1997; Evans and Kean 2002; Rogers and van Staal
98 2002; Rogers et al. 2006; van Staal 2007; Zagorevski et al. 2010). The Dunnage Zone is
99 divided into the Notre Dame Subzone, which formed near the Laurentian equatorial
100 margin, and the Exploits Subzone, which formed on the edge of Gondwana and related
101 microcontinents at mid- to high-southerly latitudes (e.g., Williams et al. 1988; Cocks and
102 Torsvik 2002; Zagorevski et al. 2006; van Staal 2007). The suture zone between these
103 two subzones is marked by the Red Indian Line, a 2-3 km wide mylonitic shear zone
104 gently dipping towards the northwest (Fig. 1; e.g. O'Brien 1991; Cocks and Torsvik
105 2002; Zagorevski et al. 2006; van Staal 2007). The Exploits Subzone is divided into four
106 geotectonic domains (Figs. 1, 2), which are: 1) the Neoproterozoic arc and back-arc
107 remnants derived from Ganderia; 2) the 513-488 Ma arc and back-arc volcanic sequences
108 of the Penobscot Arc, which hosts the Lemarchant deposit and numerous other VMS
109 deposits (Fig. 2; e.g., Duck Pond and the Boundary deposits); 3) the 473-455 Ma arc and
110 back-arc volcaniclastic and sedimentary sequences of the Popelogan-Victoria Arc, which
111 was built in part on the older Penobscot Arc; and 4) younger marine sedimentary rocks
112 covering the Popelogan-Victoria Arc sequence (Dunning and Krogh 1985; Dunning et al.
113 1987, 1991; Evans et al. 1990; Squires et al. 1991, 2001; Colman-Sadd et al. 1992;
114 O'Brien et al. 1997; MacLachlan and Dunning 1998a, 1998b; MacLachlan et al. 2001;
115 Evans and Kean 2002; Squires and Moore 2004; Rogers et al. 2006; Zagorevski et al.
116 2007b, 2010; McNicoll et al. 2008, 2010; van Staal and Barr 2012; Piercey et al. 2014).
117 These arcs and related back-arcs sequences were accreted onto the passive margin of
118 Ganderia during the Penobscot Orogeny (486-478 Ma; Colman-Sadd et al. 1992; van

119 Staal 1994; Johnson et al. 2009; Zagorevski et al. 2010), and to Laurentia during phase 3
120 of the Taconic Orogeny (~461 to ~450 Ma; Zagorevski et al. 2010; van Staal 2007; van
121 Staal and Barr 2012).

122 The Lemarchant deposit is occurs within the Victoria Lake supergroup, which
123 includes elements of both the Penobscot and Popelogan-Victoria arcs (Fig. 2). Elements
124 of the Penobscot Arc include: the 513-509 Ma bimodal volcanic rocks of the Tally Pond
125 group, which hosts the Lemarchant deposit (Dunning et al. 1991; Rogers et al. 2006;
126 McNicoll et al. 2008); the 514-506 Ma bimodal volcanic rocks of the Long Lake group
127 (Zagorevski et al. 2007a; Hinchey and McNicoll 2016); the 496.5 ± 1 Ma dominantly
128 felsic with minor mafic volcanic rocks of the Tulks group (G.R. Dunning, personal
129 communication, 2008); and the 491-488 Ma bimodal volcanic rocks of the Pats Pond
130 group (Zagorevski et al. 2007a; Hinchey and McNicoll 2009). Elements of the
131 Popelogan-Victoria Arc comprise the >465 Ma to >455 Ma dominantly sedimentary with
132 minor felsic volcanic rocks of the Noel Paul's Brook Group (Dunning et al. 1987;
133 Zagorevski et al. 2008), the 462-457 Ma sedimentary rocks of the Sutherlands Pond
134 group (Dunning et al. 1987; Zagorevski et al. 2008) and the ~453 Ma sedimentary, felsic
135 volcaniclastic and subordinate mafic volcanic rocks of the Wigwam Brook group
136 (Zagorevski et al. 2007a).

137 The Tally Pond group has been informally subdivided into two units that include
138 the predominantly mafic Lake Ambrose formation and the predominantly felsic Bindons
139 Pond formations (Rogers and van Staal 2002; Rogers et al. 2006). The Lake Ambrose
140 formation consists of vesicular to amygdaloidal, dark green to grey, massive to locally
141 pillowed tholeiitic basalt flows and subordinate tuff, pillow breccia, volcanic breccia and

142 andesitic flows. Geochemically, rocks from the Lake Ambrose formation are
143 predominantly arc tholeiites with $\varepsilon Nd_t > 0$ (Rogers et al. 2006). Felsic volcanic rocks of
144 the Bindons Pond formation comprise massive to flow-banded aphyric dacite and
145 rhyolite, quartz- and/or feldspar-phyric rhyolite, volcaniclastic, epiclastic, and crystal
146 tuff, volcanic breccia and subvolcanic quartz porphyry. Geochemically, they have calc-
147 alkalic to transitional signatures with $\varepsilon Nd_t$ ranging from +1.77 to -2.64 indicative of both
148 juvenile and evolved components in their genesis (Rogers et al. 2006). Regionally, the
149 rocks of the Lake Ambrose formation are found stratigraphically below the Bindons Pond
150 formation (Kean and Evans 1986; Evans and Kean 2002; Rogers and van Staal 2002;
151 Rogers et al. 2006) but at Lemarchant, they are found stratigraphically overlying the
152 Bindons Pond formation (Copeland 2008).

153 *2.2 Geology of the Lemarchant Deposit*

154 The Lemarchant deposit consists of two mineralised zones: the Main Zone and the
155 Northwest Zone (Fig. 3). The Main Zone contains an indicated resource of 1.24 million
156 tonnes grading at 5.38% Zn, 0.58% Cu, 1.19% Pb, 1.01 g/t Au and 59.17 g/t Ag and an
157 inferred resource of 1.34 million tonnes grading 3.70% Zn, 0.41% Cu, 0.86% Pb, 1.00 g/t
158 Au and 50.41 g/t Ag (NI43-101; Fraser et al. 2012). At present, there is no NI-43-101
159 compliant resource for the Northwest Zone. Both zones are hosted by massive felsic
160 flows of the Bindons Pond formation and are separated by a structurally complex
161 corridor. They are interpreted to represent two parts of a single dismembered sulphide
162 lens that have been displaced by the Lemarchant fault (Fraser et al. 2012). However,
163 given the structural complexity of the corridor, it is possible that these two mineralised

zones represent different mineralised lenses that were superimposed during post-VMS formation deformation.

The Main Zone ranges in thickness from 1.7 to 30.4 m, strikes south-southwest, dips shallowly towards the northwest, and is occurs near or at the contact with the conformable mafic volcanic rocks of the Lake Ambrose formation (Copeland 2008; Fraser et al. 2012; Gill 2015). The Northwest Zone ranges in thickness from 1.8 to 29.8 m, strikes northwest, dips steeply (~60°) towards the northeast (Fraser et al. 2012).

The mineralisation in both zones consists of <30 m thick lenses of massive, semi-massive, and stringers of sphalerite, chalcopyrite, galena, pyrite, pyrrhotite, and barite that precipitated in three stages (Gill et al. 2013, 2015, in press; Gill and Piercey 2014). Stage 1 is characterised by precipitation of low-Fe sphalerite and pyrite whereas Stage 2 is marked by precipitation of sulphosalts (i.e., tetrahedrite-tennantite), bornite, stromeryite, electrum, bladed barite, Ca-Fe-Mg-Mn-carbonate, and enrichments in epithermal suite elements (i.e., Au, As, Bi, Co, Cr, In, Mo, Ni, Sb, Se, Te), which are atypical of VMS deposits (Gill et al. 2013, 2015, in press; Gill and Piercey 2014). Both stages are interpreted to have formed at relatively low temperature (150-250°C) in a shallow water environment (<1500 metres below sea level (mbsl)) wherein intermitted boiling principally occurred during Stage 2 and produced the Ag and Au enrichment observed at the Lemarchant deposit (Gill et al. 2013, 2015, in press; Gill and Piercey 2014). Stage 3 consists of a late overprint of stages 1 and 2 assemblages by chalcopyrite and pyrite, and the creation of a stringer zone below the stratiform zone of the Lemarchant deposit. It is interpreted as a return to more “typical” VMS conditions, and correlate with a marked increase in the temperature of the hydrothermal fluids (>300°C).

187 Stage 3 is also associated with a deepening of the basin to >1500 mbsl due to the absence
188 of epithermal suite elements and the lack of boiling evidences (Gill et al. 2013, 2015, in
189 press; Gill and Piercey 2014).

190 A thin layer of discontinuous exhalative mudstone (<1 to 20 m) caps the massive
191 sulphide lenses and extends to four kilometres from the deposit (Copeland 2008; Fraser et
192 al. 2012; Lode et al. 2015, 2016). Hydrothermal alteration associated with the mineralised
193 zones is characterised by intense and localized Ba-enrichment, quartz, sericite and
194 chlorite hydrothermal alteration (Fraser et al. 2012). At present, the alteration associated
195 with the Lemarchant deposit has been outlined over 4 kilometres in strike and is open to
196 the north and south (Copeland 2008; Fraser et al. 2012). Post-mineralisation, possibly
197 syn-mafic volcanic, mafic and felsic dikes intrude the felsic and mafic volcaniclastic and
198 volcanic rocks of the Tally Pond group.

199 Post-mineralisation deformation of the deposit occurred along the Lemarchant
200 thrust fault (Copeland 2008; Fraser et al. 2012). Late east-southeast trending and
201 southerly dipping normal faults also displaced the Main Zone between sections 104+00N
202 and 106+00N (Fig. 3).

203 ## 3. Stratigraphic sequences

204 A total of 53 diamond drill cores from 10 sections across the Lemarchant area
205 were logged to identify and map the main structures and lithostratigraphic units present in
206 area. The volcaniclastic lithofacies described herein are classified using the classification
207 of Fisher (1966), which has been updated by
208

. These classifications are non-genetic and based entirely on clast size and abundance, with no implications for the nature or mechanism of emplacement. Lithogeochemistry is discussed in detail in the following section; however, the rock nomenclature based on immobile trace elements is presented herein for chemostratigraphic purposes. Four volcano-sedimentary sequences, one mineralised sequence, and several intrusive phases are recognised at the Lemarchant deposit. The lithological sequences from a representative drill core (LM11-51 from section 104+50N), three cross-sections from section lines 103+00N, 104+50N, and 160+00N, and a three-dimensional model of the distribution of the subsurface lithology are presented in Figures 4, 5 and 6 respectively. Overall, the lithostratigraphic sequences of the Lemarchant deposit reflect an evolution from a distal (sequences 1 and 2) volcaniclastic dominated environment of formation to a proximal (sequence 3) volcanic dominated depositional environment.

### *3.1 Sequence 1*

Sequence 1 is found at the base of the stratigraphy at the Lemarchant area and chemically falls within the basalt/andesite field of Pearce (1996) (Fig. 7a). The sequence consists of volcano-sedimentary lithofacies dominated by tuff (50%) and poorly sorted breccias (46.5%) and lapilli-tuffs (3.5%). The tuff is andesitic in composition, is grey to dark blue in colour and consists of >90% matrix with rare small (2-20 mm) monolithic clasts and flattened carbonate filled cavities (Figs. 7a, 8c). Minor <30 mm circular to elliptical, red to orange staining of the rock is also characteristic of this lithofacies.

The lapilli-tuff and breccia are grey to dark blue-green in colour and contain >50% angular to subrounded andesitic clasts. Rare subrounded to rounded basaltic clasts

and polylithic breccia clasts consisting of red chert, felsic, intermediate and mafic fragments occurs locally (Fig. 8ab), suggesting a multi-source provenance. Characteristic interstitial dark chlorite aggregates are interstitial to the clasts to the volcaniclastic rocks matrix (Fig. 8a), and likely to reflect seawater alteration of volcanic glass shards shortly after their formation. When clast-supported, the chlorite aggregates within the breccias and lapilli-tuffs may account for up to 100% of the inter-clast matrix.

Sequence 1 is constrained to the northwest and west portion of the Lemarchant area and is found in the hanging wall of the KJ and the Lemarchant shear zones, and in the footwall (north side) of the Bam fault (Figs. 5, 6).

*3.2 Sequence 2*

Sequence 2 falls within the basalt/andesite field of Pearce (1996) and consists of volcaniclastic lithofacies dominated by poorly sorted polymictic breccia (47%) and lapilli-tuffs (18%) with lesser tuff (35%) (Fig. 8a). The lapilli-tuffs and breccias are pale grey to dark grey in colour and generally contain >50% clasts. The clasts are angular to subrounded and dominated by andesitic clasts with subordinate subrounded to rounded smaller mafic and chert clasts (Figs. 7a, 8d). Unlike rocks of sequence 1, polymictic clasts and interstitial aggregate of dark chlorite are absent in the matrix of the volcaniclastic rocks of sequence 2.

The tuff of sequence 2 is macroscopically and chemically indistinguishable from those of sequence 1 (Fig. 8e), except that the tuff intervals from sequence 2 are generally restricted to a few meters compared to the 10s to 100s of meters of the tuffs of sequence 1.

Sequence 2 conformably overlies sequence 1 and is constrained to the northwest portion of the Lemarchant area. Like sequence 1, it is found in the hanging wall of the KJ and the Lemarchant shear zones, and in the footwall (north side) of the Lemarchant shear zone and Bam fault (see section 5; Figs. 5, 6). It represents a change in the clasts source with the disappearance of the polymictic clasts and dark chlorite aggregates.

*3.3 Sequence 3*

Rocks from sequence 3 are bimodal in composition and clusters within the basalt/andesite and dacite/rhyolite fields of Pearce (1996) (Fig. 7a). Both group are macroscopically similar and can only be distinguished through geochemical analysis. Andesitie ($3_I$) is dominant at the base of the sequence whereas dacite ($3_F$) is more common near the top of the sequence and are the primary host to the mineralisation (Figs. 5, 6). Both andesite and dacite consists of poorly sorted monomictic breccias and flows, and are consistent with deposition in a vent proximal depositional setting (McPhie et al. 1993; Allen et al. 1996; Gibson et al. 1999).

The monomictic breccias contains >50% very fine-grained quartz and feldspar, a dark grey to dark blue matrix, disseminated pyrite (<3%), and large (>10 cm) intermediate to felsic clasts (Fig. 8fg). They consist of aggregates of monomictic, clast-supported, matrix-poor, poorly sorted volcaniclastic rocks that commonly grade into in situ jigsaw-fit breccia and massive flows. Individual breccia intervals correlate poorly between drill holes and appear to have irregular geometries and distributions. The monomictic breccias are commonly overprinted by weak to strong sericite alteration. Veinlets of sphalerite, chalcopyrite, coarse quartz, chlorite and carbonate crosscut the monomictic breccias and early sericite alteration near mineralised intervals. However,

277 late sericite veinlets also crosscut the sphalerite-chalcopyrite veinlets, suggesting at least
278 two episodes of sericite alteration. It is unclear if the monomictic breccias are formed by
279 synvolcanic autoclastic mechanisms or are the result of hydrothermal alteration of
280 jigsaw-fit breccias on flow margins, transforming them into apparent pseudo matrix-
281 supported breccia (Allen 1988; McPhie et al. 1993).

282 The flows are flow-banded and jigsaw-fit flows that are white to creamy-yellow
283 (Fig. 8hi). The groundmass consists of an intergrowth of quartz and feldspar with
284 subordinate euhedral, <1 mm long, disseminated pyrite and anatase grains. Feldspar
285 phenocrysts <2 mm long are also present in the groundmass and locally exhibit Carlsbad
286 or albite twinning. Aphanitic dark grey to black chlorite with subordinate sphalerite, and
287 chalcopyrite fills the interstices between the jigsaw pieces. Both flows commonly display
288 varying degrees of late sericite and carbonate alteration.

289 Sequence 3 is commonly in structural contact with sequences 1 and 2 but is
290 conformable with sequence 2 in section 106+00N (Fig. 5c). Sequence 3 rocks occur in
291 every structural block at Lemarchant but are more predominant within the central and
292 western portion of the Lemarchant property (Figs. 5, 6).

293 *3.4 Mineralisation and alteration*

294 Lithofacies associated with the mineralised sequence include: exhalative
295 mudstones, massive barite, massive to semi-massive sulphides, chaotic chlorite-carbonate
296 alteration, chlorite alteration and sericite alteration. The mineralisation in both the Main
297 and Northwest zones is hosted within the dacitic breccias and flows of sequence 3, with
298 the exception of the exhalative mudstones, which overlay the rocks of sequence 3.
299 Precise timing for the initiation of the Lemarchant VMS system is not known. However,

crosscutting relationships suggest that it was initiated after the emplacement of the dacitic flows of sequence $3_F$ and prior to the deposition of the basalts of sequence 4. Layers of exhalative mudstones are also present within the hanging wall basalts above the Main Zone attesting that the Lemarchant hydrothermal system was at least still partly active during the deposition of the lowermost basalts of sequence 4.

*3.4.1 Mudstone:* The mudstones commonly vary in thickness between 0.1 and 10 m but can be as thick as 23 m. They are brown to black in colour, finely laminated, graphitic, and contain various amounts of fine carbonaceous/organic-rich laminae intercalated with chert ± apatite and with sulphides layers and are commonly hydrothermal exhalites (Fig. 9ab; Lode et al. 2015, 2016). Sulphides are dominated by pyrite and pyrrhotite, with minor amounts of marcasite, chalcopyrite, sphalerite, arsenopyrite, and galena. There is an increase in the chalcopyrite, sphalerite and galena content with proximity to the massive sulphide (Lode et al. 2015). Pyrrhotite-rich mudstones are common near the contacts with mafic intrusions and may be related to desulphidation of pyrite during the emplacement of the mafic intrusions. In general, mudstones near the Main Zone are generally well preserved but locally display weak to moderate shearing (Fig. 9a). In contrast, mudstones at the Northwest Zone are commonly structurally complex and have been affected by tight to open folding and faulting (Fig. 9b).

*3.4.2 Massive barite:* Barite-rich intervals are found below the mudstones and vary in thickness between 2 and 25 m. Barite is white to dark blue-grey in colour and occurs as granular massive barite and is locally bladed (Fig. 9c). Massive barite intervals replace the felsic and intermediate volcanic footwall rocks and is intergrown with, and

323 replaced by sulphide mineralisation (Gill and Piercey 2014; Gill et al. 2015, in press).

324 *3.4.3. Massive to semi-massive sulphides:* Massive to semi-massive sulphide
325 lenses are up to 25 m thick and consist principally of white to yellow sphalerite with
326 subordinate of pyrite, chalcopyrite and sulphosalts replacing the intermediate and felsic
327 volcanic host rocks (Fig. 9de; Gill and Piercey 2014; Gill et al. 2013, 2015, in press).
328 Semi-massive sulphides occur as disseminated aggregates and veins localised on
329 fragment margins of the jigsaw-fit fragments and along flow-banding in the more
330 massive parts of flows (Fig. 9e). Semi-massive sulphides are associated with zones of
331 moderate to strong chlorite, sericite and/or quartz alteration. Massive sulphides
332 commonly occur above semi-massive sulphide zones but can locally occur below or
333 within larger intervals of semi-massive sulphides.

334 In the Main Zone (along section 103+00N; Fig. 5a), a pipe-shaped mineralised
335 zone is observed below the dacitic volcanic rocks of sequence $3_F$ and above the
336 Lemarchant thrust in drill core LM11-61. In the Northwest Zone (along section
337 106+00N; Fig. 5c), the mineralisation occurs immediately below the LJ shear zone.

338 *3.4.4 Alteration:* Alteration in the Lemarchant deposit consists of chlorite-
339 carbonate, chlorite, sericite, and silica alteration (Fig. 9fgh). Alteration varies from weak
340 to strong and occur below the massive and semi-massive sulphide lenses. Chlorite ±
341 carbonate alteration occurs within and below the semi-massive sulphide and generally
342 overprints sericite alteration. Silica alteration occurs with both chlorite and sericite
343 alteration or by itself. Carbonate alteration occurs within the massive sulphides and also
344 extends several meters into the mafic volcanic rocks of the hanging wall.

345 *3.5 Sequence 4*

346 Sequence 4 consists of massive, pillowed, and amygdaloidal basalt and basalt
347 breccias and falls within the basalt field of Pearce (1996) (Fig. 7a). The basalts lie
348 conformably above the hydrothermal mudstones or the andesitic or dacitic volcanic rocks
349 of sequence 3. They are restricted to the eastern portion of the Lemarchant property (Figs.
350 5, 6).

351 *3.5.1 Massive basalt:* The massive basalts are aphanitic, dark grey to dark green
352 with rare 0.5-2 mm feldspar and magnetite phenocrysts (Fig. 10a). They are crosscut by
353 minor (up to 10%) 1-3 mm wide carbonate veinlets and 1-5 mm wide quartz-carbonate
354 veinlets. Epidote alteration of the matrix is rare and restricted to within or immediately
355 adjacent to fracture zones.

356 *3.5.2 Amygdaloidal basalt:* The amygdaloidal basalts are similar to the massive
357 basalts but have 5-20%, 1-20 mm wide, rounded to sub-rounded carbonate filled
358 amygdules (Fig. 10b). Chlorite replacement of carbonate in the amygdules occurs near
359 fracture zones.

360 *3.5.3 Pillow basalt:* Intervals of pillow basalts consist predominantly of 5 to 50
361 cm wide pillows with rare pillows >50 cm in width. The pillows are aphanitic, dark grey
362 to dark green, and contain 5-20% carbonate filled, 1-20 mm wide, rounded to sub-
363 rounded amygdules (Fig. 10c). The amygdules are generally smaller and more elongated
364 towards the edge of the pillow where they are 1-2 mm wide. Inter-pillow volcano-
365 sedimentary rocks consist of a mixture of very fine-grained basalt, epidote, white mica,
366 carbonate, and pyrite. The pillow basalts are crosscut by moderate amounts (up to 10%)
367 of 1-3 mm wide carbonate veinlets and 1-5 mm wide quartz-carbonate veinlets. Both the

pillows and interflow sedimentary rocks commonly have weakly to moderately developed epidote and carbonate alteration.

*3.5.4 Basalt breccia:* The basalt breccias are highly variable in texture and vary between jigsaw-fit, fragment- to matrix-supported-breccia. Fragments consist of aphanitic, dark green to dark grey basalt that vary in size between 0.5 and 10 cm (Fig. 10d). The matrix varies between carbonate dominated to epidote ± carbonate dominated.

*3.6 Intrusions*

Three types of intrusions have been identified in the Lemarchant area, including: mafic, intermediate and felsic intrusions.

*3.6.1 Mafic intrusions:* Mafic intrusions are macroscopically similar to the amygdaloidal basalts of sequence 4 and fall within the basalt field of Pearce (1996) (Fig. 7a). They are aphanitic, dark grey to dark green to grey-beige in colour, contain10-25% of 1-20 mm carbonate-filled amygdules (Fig. 11a). The mafic intrusions locally exhibit sharp chilled contact margins, which make them difficult to identify when intruding mafic extrusive rocks of sequence 4. However, the intrusions can be recognised by their significantly lower amounts (<1%) of carbonate or quartz veinlets. Likewise, the mafic intrusions and locally contain 20-40 mm long euhedral pyrite cubes which are absent in the mafic extrusive rocks. The mafic intrusions cross-cut rocks from all sequences and rare <10 m sills occur within the mafic rocks of sequence 4. Trace element composition of the mafic intrusions is indistinguishable from the mafic extrusive rocks of sequence 4 (Fig. 7), and suggests that the emplacement of the mafic intrusions might have been in part synchronous or genetically related with the deposition of the mafic volcanic rocks of sequence 4.

391 *3.6.2 Felsic intrusions:* Two types of felsic intrusions with chemistries clustering
392 within the dacite/rhyolite fields of Pearce (1996) are present at Lemarchant (Fig. 7a). The
393 first type is cream coloured and contains <20%, 2-5 mm wide, feldspar phenocrysts
394 hosted in quartz-rich groundmass that locally exhibit chilled contact margins (Fig. 11c).
395 The second type is volumetrically subordinate (<0.5% of total rock volume) and consists
396 of 20-50%, 1-3 mm long, white feldspar phenocrysts hosted in a creamy-white to pink
397 groundmass. These intrusions are commonly <5 m wide, exhibit sharp chilled margins
398 with surrounding rocks and occur within or proximal to shear zones. The felsic intrusions
399 crosscut every sequences present in the Lemarchant area, including the mineralisation
400 and alteration sequence. However, they are commonly spatially associated with the felsic
401 rocks of sequences 1 to 3 and are not volumetrically abundant in the mafic volcanic rocks
402 of sequence 4.
403 *3.6.3 Intermediate intrusions:* The intermediate intrusions contain <15%, 1-4 mm
404 wide, white feldspars phenocrysts hosted in a pale grey groundmass (Fig. 11b).
405 Intermediate intrusions are volumetrically minor, accounting for <1% of the rocks present
406 at Lemarchant. These intrusions are not spatially associated with the mineralisation and
407 are only recognised as cross-cutting bodies in sequence 4 in drill cores LM11-49 and
408 LM11-50 on section 108+00N.

409 ## 4. Lithogeochemistry

410 A total of 794 samples of all rock, alteration and mineralisation types from the
411 Lemarchant area were collected from 46 diamond drill cores. Major oxides ($SiO_2$, $Al_2O_3$,
412 $Fe_2O_3$, MnO, MgO, CaO, $Na_2O$, $K_2O$, $TiO_2$, $P_2O_5$) were analysed at ALS Global

413 following the ME-XRF06 method in which 0.9 g of sample was added to 9.0g of lithium
414 borate Flux (50% - 50% $Li_2B_4O_7 – LiBO_2$), mixed well and fused into a glass disc with an
415 auto fluxer between 1050 and 1100°C, and analysed by X-ray fluorescence spectroscopy
416 (XRF). Lower detection limits are 0.01% for all of the major oxides. Trace elements were
417 analysed on 371 samples at ALS Global following the ME-MS81 method in which 0.2 g
418 of crushed sample is added to 0.9g of lithium metaborate ($Li_2B_4O_7$), mixed well and
419 fused in a furnace at 1000°C. The resulting melt was cooled and dissolved in 100mL of
420 4% $HNO_3$ and 2% HCl solution, and was analysed by inductively coupled plasma mass
421 spectrometry (ICP-MS). Lower detection limits varied between 0.01 and 10 ppm, with
422 most elements having detection limits below 1 ppm.
423 Most host rocks in VMS systems are altered to some extent (e.g., Large, 1977;
424 Franklin et al., 1981, 2005; Lydon, 1984, 1988; Hannington, 2014), restricting the
425 elements that can be used for understanding the primary lithogeochemical signatures of
426 host rocks. Immobile elements such as Al, Ti, the high field strength elements (HFSE)
427 and the REE (except Eu) are ideal to provide information on the primary petrochemical
428 attributes of the rocks in VMS systems. However, caution must be used as some of these
429 element may become mobile (especially the LREE) during intense hydrothermal
430 alteration (MacLean, 1988).

431 *4.1 Mobile element systematics*

432 Rocks from the Lemarchant area display weak to strong alteration. Overall,
433 $Al_2O_3/Na_2O$ ratios (Fig. 12a; Spitz-Darling index, Spitz and Darling, 1978) are generally
434 lower than 20, indicating low levels of alteration, However, samples with $Al_2O_3/Na_2O$
435 ratios as high as ~50 occur in sequences $3_l$, and 4 and in the mafic intrusion. Samples

436 with $Al_2O_3/Na_2O$ ratios as high as 235 occur in sequence $3_F$, indicative of strong
437 alteration. Plot of AI index (AI = $100*(MgO+K_2O)/(MgO+K_2O+CaO+Na_2O)$; Ishikawa
438 et al., 1976) versus chlorite-carbonate-pyrite index (CCPI =
439 $100*(MgO+Fe_2O_3)/(MgO+Fe_2O_3+CaO+Na_2O)$; Large et al., 2001), rocks from sequences
440 1, 2 and 3, and the felsic intrusions plot in both the least altered and the altered fields,
441 whereas rocks from sequence 4 and the mafic intrusions plot only in the least altered field
442 (Fig. 12b). Felsic and intermediate samples that plot in the altered field display moderate
443 to high AI and CCPI indexes, and vary between the least altered, the sericite and the
444 chlorite fields. In addition, some felsic volcanic rocks from sequence 3 and felsic
445 intrusion have high $Na_2O$ values (Fig. 12a) and plot near the albite field in the AI versus
446 CCPI diagram (Fig. 12b).

447 *4.2 Immobile element systematics*

448 Most rocks fall within the tholeiitic field of Ross and Bedard (2009) (Fig. 7b)
449 with rocks from sequences 1, 2, $3_I$, 4, and the mafic intrusions defining a cluster with
450 Zr/Y ratios ranging from 1.9 to 5.3, and dacitic rocks from sequence $3_F$ defining another
451 cluster with higher Zr/Y ratios ranging from 3.2 to 5.5. Felsic intrusions have even higher
452 Zr/Y ratios ranging from 3.5 to 6.6, indicating a tholeiitic to transitional affinity (Fig. 7b).
453 The dacites of sequence 3 and the felsic intrusions plot in the volcanic arc field on the
454 Nb-Y discrimination diagram of Pearce et al. (1984) (Fig. 7c), whereas the mafic rocks of
455 sequence 4 and the mafic intrusions plot on the boundary between the island arc tholeiite
456 and the mid-ocean ridge basalt (MORB)/back-arc basalt (BAB) fields on the Ti-V
457 discrimination diagram of Shervais (1982) (Fig. 7d).

458 All the samples have low Zr (<200 ppm) and Nb (<10 ppm) contents (Fig. 7e),
459 upper crust-normalised La/Sm ratios <1 (McLennan, 2001; Fig. 7f), and are consistent
460 with input from juvenile crust/mantle (Piercey, 2010, 2011). In addition, most samples
461 fall within the FIIIa field (Fig. 7g) of Lesher et al. (1986) and Hart et al. (2004),
462 indicating that partial melting likely took place at relatively shallow levels (<10km) in the
463 crust. However, the basalts from sequence 4 and the mafic intrusions suggest crustal
464 contamination and/or slab fluid influence based on the Th/Yb-Nb/Yb discrimination
465 diagram of Pearce (2008) (Fig. 7h).

466 *4.3 Primitive mantle normalised plots systematics*

467 The extended trace element profiles for each sequence has been normalised to
468 relative to the primitive mantle values of Sun and McDonough (1989). Overall, every
469 sequence has negative Nb, Ti, and Zr anomalies (Fig. 13). Intermediate volcanic rocks of
470 sequences 1, 2 and $3_I$ have similar extended trace element profiles and are enriched in
471 light REE compare to heavy REE, with negative Nb and Ti, moderate negative Zr
472 anomalies (Fig. 13a-c). The dacite of sequence $3_F$ is enriched in light REE, has strong
473 negative Nb and Ti anomalies and moderately negative Zr anomalies (Fig. 13d). The
474 profiles are similar to the profiles of intermediate volcanic rocks from sequences 1, 2 and
475 $3_I$ but the dacite exhibits more pronounced negative Ti anomalies. Felsic intrusions have
476 similar profiles to the dacite of sequence $3_F$ but generally contain higher absolute values
477 of trace elements (Fig. 13e). Basalts from sequence 4 and the mafic intrusions have
478 similar flat extended trace element profiles, characterised by strong negative Nb
479 anomalies, and moderately negative Zr and Ti anomalies (Fig. 13fg).

## 5. Structural elements

Structural elements in the Lemarchant area consist of fractures, gouge, shear zones, and faults. Fracture zones range from 10s of centimetres to 10s of meters and consist of sharp sets of dense to widely spaced parallel fractures. The fractures are generally open with no visible alteration on their surfaces, except in rare cases where the fracture surfaces and the adjacent bedrock is bleached up to 1 cm into the wallrock. The majority of fractures have smooth surfaces indicating minimal displacement along them; however, fracture surfaces locally show slickenlines, indicating some displacement. Within the fault zones, areas with the maximum intensity of deformation manifest themselves as 5-25 cm wide zones of bleached fault gouge. Fracture zones are present in every rock unit at Lemarchant.

Shear zones consist of moderately to highly foliated ductile to brittle shears. They vary in thickness from 10 cm to 10s of meters, depending on the competence of the rocks and the deformation intensity. The main shear zones recognised during this study are termed the LJ, KJ and Lemarchant shear zones, whereas the Bam fault is the only extensional fault recognised in the study area (Fig. 6).

### *5.1 LJ shear zone*

The LJ shear zone is a southeast striking shear zone dipping at ~60° towards the southwest (Fig. 6). It typically ranges in thickness from 0.5 to 7 meters, but can locally be up to 25 m in thickness. It occurs exclusively within rocks of sequence 3 and thrusts the non- to weakly-mineralised rocks of the hanging wall over the non- to highly-mineralised rocks of the footwall. The LJ shear zone has been folded into open folds during post-VMS deformation (Fig. 6). A late mafic intrusion, herein referred to as the Pacman

503 intrusion, was emplaced in the axis of the LJ shear zone in between section 104+50N and
504 106+50N, healing and masking portions the LJ shear zone in these areas. The LJ shear
505 zone and the Pacman intrusion are cross-cut by the Lemarchant shear zone (Fig. 6).

506 *5.2 KJ shear zone*

507 The KJ shear zone is parallel to and located ~10 to 35 m above the LJ shear zone
508 (Fig. 6). The KJ shear zone varies in thickness between 0.4 and 8 meters and thrusts
509 rocks from sequences 1 and 2 over non- to weakly- mineralised rocks of sequence 3. As
510 it is the case for the LJ shear zone, the KJ shear zone has been affected by open folding
511 during post-VMS event deformation, and was intruded by the Pacman intrusion between
512 sections 104+50N and 106+50N is crosscut by the Lemarchant shear zone (Fig. 6).

513 *5.3 Lemarchant shear zone*

514 The Lemarchant shear zone is an extensive, relatively flat, horizontal shear zone
515 that occurs throughout the Lemarchant property (Fig. 6). On average, it ranges between 1
516 and 10 m in thickness but is locally up to 30 m thick. The Lemarchant shear zone is offset
517 by the Bam fault in the central portion of the property between section 104+00N and
518 105+00N. The observed depth of the Lemarchant shear zone is approximately 200 m
519 above the mean sea level north of the Bam fault and 100 m above the mean sea level
520 south of the Bam fault. The Lemarchant shear zone is not significantly affected by
521 folding and crosscuts both the LJ and KJ shear zones.

522 *5.4 Bam fault*

523 The Bam fault is an east striking fault dipping at ~60° towards the south and
524 ranges in thickness between 1-10 m (Fig. 6). It crosscuts the LJ, KJ and Lemarchant shear

zones. The Bam fault records a normal-sense of displacement wherein the rocks south side of the fault was down-faulted relative to the north side. Relative movement is estimated to be around 100 to 150 meters based on the offset of the Lemarchant shear zone (Fig. 6).

## 6. Discussion

### *6.1 Tectonic Evolution of the Lemarchant Host Rocks*

All sequences and intrusions examined in this study exhibit similar primitive mantle normalised extended REE profiles with negative Nb, Zr, and Ti anomalies (Fig. 13), suggesting a similar tectonic environment of formation. In general, negative Nb, Zr, and Ti anomalies are characteristic of "arc" environments, where slab metasomatism has influenced the overlying mantle wedge resulting in an enrichment of large ion lithophile elements relative to high field strength elements (e.g. Hawkesworth et al 1993; Pearce and Peate, 1995; Piercey, 2010). This "arc" signature is also supported in the Ti-V systematic of the basalts and mafic intrusions (Fig. 7d), where they cluster near the boundary between the island arc and back-arc/MORB fields. Additional support for the "arc" signature can be seen in Th/Yb and Nb/Yb discrimination diagram where basalt and mafic intrusions plots above the MORB-OIB array with elevated Th/Yb at a given Nb/Yb (Fig. 7h), indicating either the influence from slab metasomatism or crustal contamination during ascent. In addition, the dacite and felsic intrusions plot in the volcanic arc field on the Y versus Nb discrimination diagram of Pearce et al. (1984) (Fig 7c), further supporting the arc environment interpretation.

547 Despite the evidence for an arc environment, the majority of the Lemarchant
548 samples have a tholeiitic affinity (Fig. 7b), exhibit juvenile signatures compare to typical
549 upper continental crust ($La/Sm_{UCN}$ <1; Fig. 7f) and plots in the post-Archean juvenile
550 VMS environment field on the Nb versus Zr discrimination diagram of Piercey (2011)
551 (Fig. 7e). Furthermore, the rocks at the Lemarchant area do not exhibit a continuous
552 spectrum of magmatic products, features common in most "arc" environments (e.g.,
553 Tatsumi and Eggins, 1995), but rather are bimodal to trimodal in nature, features
554 commonly observed in rifted arc environments (e.g., Vivallo and Claesson, 1987, Wright
555 et al., 1996), and consistent with regional tectonics models (e.g,. Rogers et al., 2006;
556 Zagorevski et al., 2010; Piercey et al., 2014). However, it should be noted that some areas
557 of the Tally Pond group (e.i., West and South Tally Pond zones) exhibit a continuous
558 spectrum of magmatic products fractionation (Pollock 2004). The FIIIa signature of the
559 dacite and felsic intrusions at the Lemarchant area (Fig. 7g) supports a shallow melting
560 environment (<10km), with melting taking place under low pressure (<0.5Gpa) and high
561 temperature (900-1000°C) (Fig. 7e; Lesher et al., 1986; Hart et al., 2004; Piercey, 2011).
562 Similarly, the extended REE profiles normalised to N-MORB and Ti suggest shallow
563 melting from a garnet free and spinel stable residue for the basaltic melts of sequence 4
564 (Fig. 13h; e.g., McKenzie and Bickle, 1988; McKenzie and O'Nions, 1991; Pearce,
565 2008). Therefore, the arc signatures present at Lemarchant area are interpreted to be the
566 direct result of slab metasomatism (e.g., Hawkesworth et al., 1993; Pearce and Peate,
567 1995), and/or inherited from contamination via arc crust (e.g., Morris et al., 2000) or
568 continental crust assimilation (e.g., Piercey et al., 2004). The interpreted volcano-

569 sedimentary environment at the Lemarchant area and the regional tectonic models and are
570 consistent with continental crust assimilation during magma ascent.
571 The Tally Pond group is underlain by the 563 Ma Sandy Brook group, which
572 consists of rhyolite, andesite and basalt (tholeiitic and calc-alkaline), and minor
573 siliciclastic rocks, including black shale and chert horizons (Rogers et al., 2006). These
574 rocks have evolved Nd isotopic signatures ($\varepsilon Nd_{563Ma}$ from −5.18 to −0.67) and are
575 interpreted to have formed within a continental arc environment (Rogers et al., 2006;
576 Zagorevski et al., 2010). Evidence of relatively young, but evolved crust beneath the
577 Tally Pond group at the Lemarchant deposit is also found in the Pb isotopic signatures of
578 galena from the mineralised zones (Gill et al., 2105; Gill, 2015). Therefore, it is plausible
579 that the "arc" signatures present in some of the rocks were at least in part inherited from
580 interaction with the underlying arc basement (i.e., the Sandy Brook group). Despite being
581 underlain by young arc crust, the presence of arc tholeiitic rocks with "juvenile" like
582 signatures is indicative of the magmas erupting rapidly with limited interaction with crust
583 during its ascent and is consistent with rifted arc and VMS formation environments (e.g.,
584 Piercey, 2011).
585 Several models have been proposed for the tectonic setting for the Tally Pond
586 group. Dunning et al. (1991) argued that the Tally Pond group was the product of arc
587 volcanism created by subduction zone magmatism in an oceanic setting. Rogers et al.
588 (2006) claimed that the Tally Pond belt formed from subduction along the peri-
589 Gondwanan side of Iapetus. However, they argue that the Tally Pond volcanic arc was
590 built on the Ganderian microcontinent (Sandy Brook group – Cripplebeck Intrusive Suite
591 crust) and not in an oceanic setting as proposed by Dunning et al. (1991). Based on Nd

isotopes, Rogers et al. (2006) proposed that the Tally Pond belt formed from 60% juvenile depleted mantle and 40% recycling of older crust. In contrast, Zagorevski et al. (2010) hypothesised that the arc signature of the Tally Pond belt was the result of eastward subduction creating local arc volcanism within a greater extensional back-arc complex in which the magmatic front migrated westward with time due to slab rollback. In this model, these extensional eruptive complexes are associated with longitudinal rifts crosscut by cross-arc seamount chains. Similarly, Piercey et al., (2014) argues that the Duck Pond and Boundary deposits formed within a rifted arc environment along the edge of the Ganderian margin of the Iapetus ocean. More recently, Lode et al., (2016) suggested a two-phase rifting model for the Tally Pond group wherein the Lemarchant deposit formed at shallow depth during phase one of rifting.

Our model for the Lemarchant area agrees with the young rifted arc environment of Zagorevski et al. (2010), Piercey et al. (2014) and Lode et al., (2016) and explain the abundance of rocks with a juvenile geochemical signatures, the distinctly trimodal signature of the belt comparatively to dominantly andesitic with continuous fractionation trends (basalt to rhyolite) for continental arcs (e.g., Arculus, 1994; Lentz, 1998; Swinden, 1996), and is consistent with the extensional environment of formation of VMS deposits comparatively to compressive environments for arcs (Fig. 14) (e.g. Franklin et al., 2005; Galley et al., 2007; Piercey, 2010; Piercey, 2011; Hannington, 2014). However, since continuous magmatic products are observed within the Tally Pond group (Pollock 2004), compressive arc environments were also locally present.

Due to the high abundance of andesite compared to the bimodal (basalt and rhyolite) sequence at Duck Pond and elsewhere in the Tally Pond belt (Fig. 14c), we

propose that the Lemarchant deposit formed either at an arc front or within a migrating cross-arc. A similar tectonic environment has been observed by Wright et al. (1996) within the modern Havre Through, north of the Taupo Volcanic Zone, wherein east-west andesitic arcs and associated cross-arcs occur perpendicular to the main north-south arc axis. Wright et al. (1996) suggested that the cross-arcs formed during the eastward migration of the subduction and associated arc magmatic fronts, and highlight areas where andesitic arc magma supply is greater than the rifting rate. Following this model, we hypothesise that the Lemarchant deposit formed following the attenuation of the andesitic arc magma supplies, likely when the rift-related magma supply became dominant. This transition was accompanied by a change from andesitic to dacitic magmatic composition during deposition of sequence 3 due to either mixing of the andesitic arc magma with rhyolitic magmas derived from the rift component or by crustal assimilation within the andesitic arc or cross-arc, creating the sparse dacite that host the VMS mineralisation. Subsequent to the transition to a rift dominated environment, the basalts of sequence 4 erupted over the andesitic and dacitic rocks of sequence 3. Hydrothermal activity related to the Lemarchant deposit continued during that time (i.e.., post-VMS formation) as attested by the presence of interlayered exhalative mudstones within the basalts (Lode et al. 2015, 2016).

The relatively shallower position of VMS systems formed at the front of or within the magmatic cross-arcs compared to those formed at greater depths (i.e., in rift basins) may have enhanced boiling and allow enrichment in precious metals. At Lemarchant, potential boiling is evidenced by abundant sulphosalts (i.e., tetrahedrite-tennantite), electrum, bladed barite, Ca-Fe-Mg-Mn-carbonate, and enrichments in epithermal suite

638 elements (i.e., Au, As, Bi, Co, Cr, In, Mo, Ni, Sb, Se, Te; Gill et al. 2013, 2015; Gill and
639 Piercey 2014; Lode et al., 2015). Based on the ore mineralogy of the Main Zone at
640 Lemarchant, Gill et al. (2015, in press) suggested that the deposit formed from
641 intermittent boiling of hydrothermal–magmatic fluids at relatively shallow (<1500 m)
642 water depth, and is consistent with the model propose therein. Boiling of Au-bearing
643 magmatic fluids may have aided or may have been critical to the precious metal
644 enrichment at the Lemarchant VMS system. Boiling resulted in a fluid phase with
645 decreased $HS^-$ activity due to strong fractionating of $H_2S$ into the vapour phase, increased
646 pH as a result of acidic components fractionating into the vapour phase, and decreased
647 temperature (William-Jones et al., 2009). These promotes the destabilisation of the
648 precious and base metal complexes in solution and result in their precipitation at the site
649 of boiling.

650 *6.2 Structural Evolution of the Lemarchant Area*

651 The Lemarchant area was affected by several episodes of deformation following
652 the deposition of sequences 1 to 4 and the VMS mineralisation hosted therein. Recorded
653 deformation is more intense within the mudstone near the shear zones and within sheared
654 massive sulphides of the Northwest Zone. It is proposed that the LJ and KJ shear zones
655 originated as are syn-volcanic structures as both shear zones are found at ~45° to the
656 stratigraphy (Fig. 5c), and have different geometry (affected by early folding) compared
657 to regional thrust faults in the area (Figs. 5c, 6, 15; e.g., McNicoll et al. 2010; Zagorevski
658 et al. 2010). The kinematic indicators of the LJ and KJ shear zones suggest that older
659 rocks of sequences 1 and 2 are thrusted over younger rocks of sequence 3 and records an
660 overall net reverse motion, indicating late reactivation of the syn-volcanic faults (Figs.

661 5c, 6, 13). Within the LJ shear zone, red sphalerite crosscut intervals of massive fine-
662 grained, honey brown sphalerite and chalcopyrite, and is spatially associated with small
663 aggregates of rounded to subrounded chalcopyrite. These textural relationships indicate
664 that sphalerite deformed ductily and was remobilised parallel to LJ and KJ shear zones,
665 whereas chalcopyrite was mechanically transported and concentrated into aggregates, as
666 sphalerite does not require as high a pressure/temperature, relative to chalcopyrite, to
667 reach the brittle-ductile transition and be ductily remobilised (Marshall and Gilligan
668 1987). Consequently, from the sulphide relationship observed, it can be estimated that the
669 pressures and temperatures reached during the deformation of the Lemarchant area did
670 not exceed 175 MPa and 200ºC, respectively (Marshall and Gilligan 1987).The high
671 angle LJ and KJ syn-volcanic shear zones are crosscut by the relatively flat-laying
672 Lemarchant shear zone (Figs. 5, 6, 13b) and suggests that the two mineralised zones did
673 not originate from the same lens prior to deformation (Figs. 5, 6). These observations are
674 in agreement with those compiled by Squires and Hinchey (2006), suggesting that the
675 Lemarchant shear zone is a thrust fault. On a regional scale, the Lemarchant thrust zone
676 terminates against felsis rocks of the Bindons Pond formation which are crosscut by the
677 nearby 465 ± 1 Ma (U–Pb zircon; Pollock 2004) Harpoon Hill gabbro (Squires and
678 Hinchey 2006) and possibly constrains the timing of the main deformation phases to the
679 Penobscot orogeny (486-478 Ma; Colman-Sadd et al. 1992; van Staal 1994; Johnson et
680 al. 2009; Zagorevski et al. 2010). In the eastern portion of the Exploits Subzone, east of
681 the Tally Pond group, the Penobscot orogeny was accompanied by thrusting of locally
682 derived Penobscot back-arc basin ophiolites onto the passive margin of Ganderia
683 (Colman-Sadd 1985; Colman-Sadd et al. 1992; Jenner and Swinden 1993; Zagorevski et

684 al. 2010). It is suggested that the Penobscot orogeny coincided with a NW-SE
685 compression event in the Lemarchant area, that resulted in thrusting rocks over a few
686 kilometres, as is the case for the obducted ophiolites in the east of the Exploits Subzone,
687 and was accompanied by folding of the LJ and KJ syn-volcanic shear zones (Fig 15b;
688 Colman-Sadd 1985; Jenner and Swinden 1993; Zagorevski et al. 2010).

689 The last deformation event recorded in the Lemarchant area corresponds to an
690 episode of extension marked by the creation of the west striking Bam normal fault (Figs.
691 4, 15c). Regional mapping compilation conducted by Squires and Hinchey (2006) and
692 logging of drill core south of the Main Zone suggests that the Bam normal fault is part of
693 a series of NW-SE striking late normal faults that affected the southwest and northeast
694 parts of the Tally Pond group. The timing of the late normal faults is unclear; however
695 McNicholl et al. (2010) argues that late normal faults at Duck Pond displace a gabbro
696 intrusion with a chemical signature similar to the Harpoon Hill Gabbro from which an
697 age younger than 465 Ma can be inferred for the late normal faults. By analogy, the late
698 relative timing for the normal faults at Lemarchant may suggests a maximum age of 465
699 Ma for normal faults, potentially related to an episode of tectonic relaxation post-
700 Penobscot orogeny.

701 *6.3 Implications for VMS exploration*

702 Exploration for VMS deposits in accretionary orogenic belts is challenging due to
703 post-VMS tectonic imbrication of original basin sequences (e.g., Calon and Green, 1987;
704 McClay 1995; Thurlow 1996; Nelson 1997; Castroviejo et al. 2011), and other
705 complication factors such as poor exposure, thick soil cover, or poorly understood
706 stratigraphic relationships. The work presented herein provides an approach that may be

707 useful for more effective exploration for VMS deposits in imbricated terranes worldwide.
708 The results illustrate the importance of multi-faceted approach (structural, stratigraphic
709 and chemostratigraphy) to formulate tecto-stratigraphic reconstructions. This approach
710 can help to identify disparate sulphide lenses (e.g., Northwest vs. Main zones), from
711 continuous lenses offset by faults – critical for both exploration and mine planning.
712 Furthermore, fault reconstruction illustrates that while many blocks were lithologically
713 similar (e.g., sequences 1 and 2 vs. sequence 3), they can have distinct structural
714 positions, and may have markedly different economic potential. Consequently,
715 reconstruction of poly-deformed deposits such as presented herein are not only critical to
716 understand the genesis of ancient deposits and their tectonic setting, but also for guiding
717 exploration in deposit-proximal areas. The potential of the later can be further enhanced
718 by the addition of other information layer (e.g.: geochemistry, geophysics, hyperspectral
719 reflectance) within a known geological context, which is key to efficient exploration.

720 ## 7. Conclusions

721 The Lemarchant area is underlain by four volcano-sedimentary sequences, one
722 mineralised sequence, and several intrusive phases. Sequences 1 and 2 consist of
723 andesitic breccias, lapilli-tuff and tuff and represent vent-distal volcaniclastic sequences
724 relative to the depositional centre. Sequence 3 consists of vent-proximal andesitic to
725 dacitic autoclastic volcaniclastic and associated massive flows that host the VMS
726 mineralisation. The mineralisation sequence includes exhalative mudstones, massive
727 barite, massive to semi-massive sulphides, chaotic chlorite-carbonate alteration, chlorite
728 alteration and sericite alteration and is principally hosted within the dacitic breccias and

729 flows of sequence 3, with the exception of the exhalative mudstones, which overlay the
730 rocks of sequence 3. Sequence 4 consists of tholeiitic basalts that were deposited
731 conformably on rocks of sequence 3 or on the exhalative mudstone of sequence 3. These
732 sequences are intruded by younger, possibly syn-sequence 4, felsic, intermediate and
733 mafic dikes.

734 The Lemarchant deposit consists of two distinct VMS lenses that formed within
735 massive dacitic flows and related autoclastic volcaniclastic rocks of sequence 3 that have
736 recorded different deformation styles. The Northwest Zone is hosted in the immediate
737 footwall of the folded LJ syn-volcanic shear zone, whereas the Main Zone occurs in the
738 relatively undeformed hanging wall of the Lemarchant thrust. It is proposed that the
739 tectono-stratigraphic environment of formation of the Lemarchant deposit is within a
740 shallow (<1500m below sea level) arc or migrating cross-arc seamount chain which
741 produced abundant amount of andesitic rocks. The VMS mineralisation occurs within late
742 dacitic flows (513-509 Ma) that formed during the transition between arc dominated and
743 rift dominated environment. The shallow position of the deposit promoted boiling near or
744 at the seafloor, ultimately resulting in precious metals enrichment of the Lemarchant
745 deposit. It is suggested that arcs or cross-arcs within rifted arc environment represent
746 favourable exploration targets for precious metal enriched VMS deposits.

747 Deformation of the Lemarchant deposit likely occurred during the Penobscot
748 orogeny (486-478 Ma) and coincided with the deformation of the LJ and KJ syn-volcanic
749 shear zone and subsequent creation of the Lemarchant thrust during a NW-SE
750 compression episode. The late (< 465 Ma) east trending Bam normal fault affected the

central portion of the Lemarchant area and lowered the southern portion relative to the northern portion of the studied area.

This study of the Lemarchant deposit resulted in the reconstruction of the original volcanic and structural environment, and has implications for ongoing exploration at Lemarchant and can be used as a framework for other datasets (e.g., geochemistry, geophysics, hyperspectral). The approaches and results presented in this paper are relevant to and can be utilised for understanding and exploring for VMS mineralisation in the Tally Pond group and in similar accretionary orogens globally.

## 8. Acknowledgements

Financial support for this project was provided from a Natural Sciences and Engineering Research Council of Canada (NSERC) Collaborative Research and Development Grant to S.J. Piercey. Additional funding was provided by the NSERC-Altius Industrial Research Chair in Mineral Deposits (supported by NSERC, Altius Resources Inc., and the Research and Development Corporation of Newfoundland and Labrador) and an NSERC Discovery Grant to S.J. Piercey. Logistical support was provided by Canadian Zinc Corporation. Diane Fost and Alexandria Marcotte are thank for their incredible support during the field campaigns. Jim Walker and John Hinchey are thanked for their constructive criticism and reviews of the manuscript.

## 9. References


Allen, R.L., 1988, False pyroclastic textures in altered silicic lavas, with implications for volcanic-associated mineralization. Economic Geology, v. 83, p. 1424–1446.

Allen, R.L., Ludström, L., Ripa, M., Simeonov, A., Christofferson, H., 1996, Facies analysis of a 1.9 Ga, continental margin, back-arc, felsic caldera province with diverse Zn-Pb-Ag-(Cu-Au) sulphide and Fe oxide deposits, Bergslagen region, Sweden. Economic Geology, v. 91, p. 979–1008.

Arculus, R.J., 1994, Aspects of magma genesis in arcs. Lithos, v. 33, p. 189–208.

Calon, T. J., and Green, F. K., 1987, Preliminary results of a detailed structural analysis of the Buchans Mine area. Paper - Geological Survey of Canada, v. 86–24, p. 273–288.

Castroviejo, R., Quesada, C., and Soler, M., 2011, Post-depositional tectonic modification of VMS deposits in Iberia and its economic significance: Mineralium Deposita, v. 46, p. 615–637.

Cocks, L.R.M., and Torsvik, T.H., 2002, Earth geography from 500 to 400 million years ago; a faunal and palaeomagnetic review. Journal of the Geological Society of London, v. 159, Part 6, p. 631–644.

Colman-Sadd, S.P., 1985, Geology of the Burnt Hill Map Area (2D/5), Newfoundland. Mineral Development Division, Department of Mines and Energy, Government of Newfoundland and Labrador, Report 85–3, 94 p., scale 1:50,000.

Colman-Sadd, S.P., Dunning, G.R., and Dec, T., 1992, Dunnage-Gander relationships and Ordovician orogeny in central Newfoundland; a sediment provenance and U/Pb age study. American Journal of Science, v. 292, no. 5, p. 317–355.

794 Copeland, D., 2008, The South Tally Pond project: a high-grade polymetallic VMS
795 discovery. Atlantic Geology, v. 45, p. 55.
796 Dunning, G.R. and Krogh, T.E., 1985, Geochronology of ophiolites of the Newfoundland
797 Appalachians. Canadian Journal of Earth Sciences, v. 22, p. 1659–1670.
798 Dunning, G.R., Swinden, H.S., Kean, B.F., Evans, D.T.W., and Jenner, G.A., 1991, A
799 Cambrian island arc in Iapetus: geochronology and geochemistry of the Lake
800 Ambrose Volcanic Belt, Newfoundland Appalachians. Geological Magazine, v.
801 128, p. 1–17.
802 Dunning, G.R., Kean, B.F., Thurlow, J.G., and Swinden, H.S., 1987, Geochronology of
803 the Buchans, Roberts Arm, and Victoria Lake Groups and Mansfield Cove
804 complex, Newfoundland. Canadian Journal of Earth Sciences, v. 24, no. 6, p. 1175–
805 1184.
806 Evans, D.T.W., and Kean, B.F., 2002, The Victoria Lake supergroup, central
807 Newfoundland – its definition, setting and volcanogenic massive sulphide
808 mineralization. Newfoundland and Labrador Department of Mines and Energy,
809 Geological Survey, Open File NFLD/2790. 68 p.
810 Evans, D.T.W., Kean, B.F., and Dunning, G.R., 1990, Geological studies, Victoria Lake
811 Group, central Newfoundland. Government of Newfoundland and Labrador
812 Department of Mines and Energy, Geological Survey, Report 90-1, p. 131–144.
813 Fisher, R.V., 1966, Rocks composed of volcanic fragments and their classification. Earth
814 Science Reviews, v. 1, p. 287–298.
815 Franklin, J. M., Gibson, H. L., Galley, A. G., and Jonasson, I. R., 2005, Volcanogenic
816 massive sulfide deposits. In Hedenquist, J. W., Thompson, J. F. H., Goldfarb, R. J.,

and Richards, J. P., (eds.), Economic Geology 100th Anniversary Volume. Society of Economic Geologists, p. 523–560.

Franklin, J.M., Lydon, J.W., and Sangster, D.F., 1981, Volcanic-associated massive sulfide deposits. In: Skinner, B.J. (ed.), 75th Anniversary Volume of Economic Geology. Lancaster, p. 485-627.Hannington, M.D., 2014, Volcanogenic massive sulfide deposits, In: Holland, H.D., and Turekian, K.K (eds.), Treatise on Geochemistry (Second Edition), Elsevier, Oxford, p. 463–488.

Fraser, D., Giroux, G.H., Copeland, D.A., and Devine, C.A., 2012, Technical Report and Resource Minerals Estimate on the Lemarchant Deposit, South Tally Pond VMS Project, Central Newfoundland, Canada. Paragon Mineral Corporation, Technical Report NI43–101, 132 p.

Galley, A.G., Hannington, M.D., and Jonasson, I.R., 2007, Volcanogenic massive sulphide deposits. *In* Goodfellow, W.D., ed., Mineral Deposits of Canada: A Synthesis of Major Deposit-Types, District Metallogeny, the Evolution of Geological Provinces, and Exploration Methods. Geological Association of Canada, Mineral Deposits Division, Special Publication No. 5, p. 141–161.

Gibson, H.L., Morton, R.L., and Hudak, G.J., 1999, Submarine volcanic processes, deposits, and environments favorable for the location of volcanic-associated massive sulphide deposits. *In:* Barrie, C.T., and Hannington, M.D. (eds), Volcanic-associated massive sulphide deposits: Progress and examples in modern and ancient settings. Reviews in economic geology 8, p. 13–51.

838 Gill, S.B., 2015, Mineralogy, metal zoning, and genesis of the Zn-Pb-Ba-Ag-Au
839 Lemarchant volcanogenic massive sulphide (VMS) deposit, Unpublished M.Sc.
840 thesis, St. John's, Newfoundland, Memorial University of Newfoundland, 167 p.
841 Gill, S.B., and Piercey, S.J., 2014, Preliminary mineralogy of barite-associated sulphide
842 mineralization in the Ordovician Zn-Pb-Cu-Ag-Au Lemarchant volcanogenic
843 massive sulphide deposit, Newfoundland and Labrador. Current Research -
844 Geological Survey of Canada, 2013–17: 15 p.
845 Gill, S.B., Piercey, S.J., Layton-Matthews, D., *in press*. Mineralogy and metal zoning of
846 the Lemarchant Zn-Pb-Cu-Au-Ag volcanogenic massive sulfide (VMS) deposit,
847 Newfoundland. The Canadian Mineralogist.
848 Gill, S.B., Piercey, S.J., Layton-Mattews, D., Layne, G.D., and Piercey, G., 2015,
849 Mineralogical, sulphur, and lead isotopic study of the Lemarchant Zn-Pb-Cu-Ag-
850 Au-VMS deposit: Implications for precious-metal enrichment processes in the
851 VMS environment. *In:* Peter, J.M. and Mercier-Langevin, P. (eds.), Targeted
852 Geoscience Initiative 4: Contributions to the Understanding of Volcanogenic
853 Massive Sulphide Deposit Genesis and Exploration Methods Development;
854 Geological Survey of Canada, Open File 7853, p. 183–195.
855 Gill, S.B., Piercey, S.J., and Devine, C.A., 2013, Preliminary mineralogy of barite-
856 associated sulphide mineralization in the Ordovician Zn-Pb-Cu-Ag-Au Lemarchant
857 volcanogenic massive sulphide deposit, Newfoundland and Labrador. Geological
858 Survey of Canada, Current Research, Report 2013–17, 15 p.
859 Hannington, M.D., 2014, Volcanogenic massive sulfide deposits, *In* Holland, H.D., and
860 Turekian, K.K (eds.), Treatise on Geochemistry (Second Edition), Elsevier, Oxford,

p. 463–488.

Hawkesworth, C.J., Gallagher, K., Hergt, J.M., and McDermott, F., 1993, Mantle and slab contributions in arc magmas. Annual Reviews in Earth and Planetary Science, v. 21, p. 175–204.

Hart, T.R., Gibson, H.L., and Lesher, C.M., 2004, Trace element geochemistry and petrogenesis of felsic volcanic rocks associated with volcanogenic massive Cu–Zn–Pb sulfide deposits. Economic Geology, v. 99, p. 1003–1013.

Hibbard, J., van Stall, C., Rankin, D., and Williams H., 2004, Lithotectonic Map of the Appalachian Orogen, Canada-United States of America. Geological Survey of Canada Map 2096A, scale 1:500,000.

Hinchey, J.G., and McNicoll, V., 2016. The Long Lake Group: An update on U-Pb geochronological studies. Newfoundland Geological Survey Current Research, Report 16-1, p. 27–38.

Hinchey, J.G., and McNicoll, V., 2009, Tectonostratigraphic architecture and VMS mineralization of the southern Tulks volcanic belt: New insights from U-Pb geochronology and lithogeochemistry. Newfoundland Geological Survey Current Research, Report 09–1, p. 13–42.

Ishikawa, Y., Sawaguchi, T., Ywaya, S., and Horiuchi, M., 1976, Delineation of prospecting targets for Kuroko deposits based on modes of volcanism of underlying dacite and alteration halos. Mining Geology, v. 26, p. 105–117.

Jenner, G.A., and Swinden, H.S., 1993, The Pipestone Pond complex, central Newfoundland; complex magmatism in an eastern Dunnage zone ophiolite. Canadian Journal of Earth Sciences, v. 30, no. 3, p. 434–448.

884 Johnson, S.C., McLeod, M.J., Fyffe L.R., and Dunning, G.R., 2009, Stratigraphy,
885 geochemistry, and geochronology of the Annidale and New River belts, and the
886 development of the Penobscot arc in southern New Brunswick. *In*: G.L. Martin
887 (ed.), Geological Investigations in New Brunswick for 2008. New Brunswick
888 Department of Natural Resources, Minerals, Policy, and Planning Division, Mineral
889 Resource Report 2009-2, p. 141–218.
890 Kean, B.F., and Evans, D.T.W., 1986, Metallogeny of the Tulks Hill Volcanics, Victoria
891 Lake Group, central Newfoundland. Government of Newfoundland and Labrador,
892 Department of Mines and Energy, Mineral Development Division. Report 86–1, p.
893 51–57.
894 Kean, B.A., Evans, D.T.W., and Jenner, G.A., 1995, Geology and mineralization of the
895 Lushs Bight Group. Newfoundland Department of Natural Resources, Report 95–2,
896 227 p.
897 Large, R.R., 1977, Chemical evolution and zonation of massive sulfide deposits in
898 volcanic terrains. Economic Geology, v. 72, p. 549–572.
899 Large, R.R., Gemmell, J.B., Paulick, H., and Huston, D.L., 2001, The alteration box plot:
900 A simple approach to understanding the relationships between alteration
901 mineralogy and lithogeochemistry associated with VHMS deposits. Economic
902 Geology, v. 96, p. 957–971.
903 Lentz, D.R., 1998, Petrogenetic evolution of felsic volcanic sequences associated with
904 Phanerozoic volcanic-hosted massive sulfide systems: The role of extensional
905 geodynamics. Ore Geology Reviews, v. 12, p. 289–327.
906 Lesher, C.M., Goodwin, A.M., Campbell, I.H., and Gorton, M.P., 1986, Trace element

907 geochemistry of ore-associated and barren felsic meta-volcanic rocks in the
908 Superior province, Canada. Canadian Journal of Earth Sciences, v. 23, p. 222–237.
909 Lizasa, K., Fiske, R.S., Ishizuka, O., Yuasa, M., Hashimoto, J., Ishibashi, J., Naka, J.,
910 Horii, Y., Fujiwara, Y., Imai, A, and Koyama, S., 1999, A Kuroko-type
911 polymetallic sulphide deposit in a submarine caldera. Science, v. 283, p. 975–977.
912 Lode, S., Piercey, S.J., and Squires, G.C., 2016, Role of metalliferous mudstones and
913 detrital shales in the localization, genesis, and paleoenvironment of volcanogenic
914 massive sulphide deposits of the Tally Pond volcanic belt, central Newfoundland,
915 Canada. Canadian Journal of Earth Sciences, v. 53, no. 4, p. 387–425.
916 Lode, S., Piercey, S., and Devine C.A., 2015, Geology, Mineralogy, and
917 Lithogeochemistry of Metalliferous Mudstones Associated with the Lemarchant
918 Volcanogenic Massive Sulphide Deposit, Tally Pond Belt, Central Newfoundland:
919 Economic Geology, v. 110, p. 1835–1859.
920 Lydon, J.W., 1984, Volcanogenic massive sulphide deposits Part I: A descriptive model.
921 Geoscience Canada, v. 11, p. 195–202.
922 Lydon, J.W., 1988, Volcanogenic massive sulphide deposits Part 2: Genetic models.
923 Geoscience Canada, v. 15, p. 43–65.
924 MacLachlan, K., O'Brien, B.H., and Dunning, G.R., 2001, Redefinition of the Wild Bight
925 Group, Newfoundland; implications for models of island-arc evolution in the
926 Exploits Subzone: Canadian Journal of Earth Sciences, v. 38, no. 6, p. 889–907.
927 MacLachlan, K., and Dunning, G.R., 1998b, U-Pb ages and tectonomagmatic
928 relationships of Middle Ordovician volcanic rocks of the Wild Bight Group,

929 Newfoundland Appalachians. Canadian Journal of Earth Sciences, v. 35, p. 998–
930 1017.
931 MacLachlan, K., and Dunning, G., 1998a, U-Pb ages and tectonomagmatic relationships
932 of early Ordovician low-Ti tholeiites, boninites and related plutonic rocks in central
933 Newfoundland, Canada. Contributions to Mineralogy and Petrology, v. 133, no. 3,
934 p. 235–258.
935 MacLean, W.H., 1988, Rare earth element mobility at constant inter-REE ratios in the
936 alteration zone at the Phelps Dodge massive sulphide deposit, Matagami, Quebec.
937 Mineralium Deposita, v. 23, p.231–238.
938 Marshall, B., and Gilligan, L.B., 1987, An introduction to remobilization: Information
939 from ore-body geometry and experimental considerations. Ore Geology Reviews,
940 v. 2, p. 87–131.
941 McClay, K.R., 1995, The geometries and kinematics of inverted fault systems: a review
942 of analogue model studies. *In:* Buchanan, J.G. and Buchanan, P.G. (eds.), Basin
943 inversion. Geological Society Special Publication, v. 88, p. 97–118.
944 McDonough, W.F., and Sun, S., 1995, Composition of the earth. Chemical Geology, v.
945 120, p. 223–253.
946 McKenzie, D., Bickle, M.J., 1988. The volume and composition of melt generated by
947 extension of the lithosphere. J. Petrol. 29, 625–679.
948 McKenzie, D., O'Nions, R.K., 1991. Partial melt distributions from inversion of rare
949 earth element concentrations. J. Petrol. 32, 1021–1091.

McLennan, S.M., 2001, Relationships between the trace element composition of sedimentary rocks and upper continental crust. Geochemistry Geophysics Geosystems, v. 2, 24 p.

McNicoll, V., Squires, G., Kerr, A., and Moore, P., 2010, The Duck Pond and Boundary Cu-Zn deposits, Newfoundland: New insights into the ages of host rocks and the timing of VHMS mineralization. Canadian Journal of Earth Sciences, v. 47, p. 1481–1506.

McNicoll, V., Squires, G.C., Kerr, A., and Moore, P.J., 2008, Geological and metallogenic implications of U-Pb zircon geochronological data from the Tally Pond area, central Newfoundland. Newfoundland and Labrador Department of Natural Resources, Geological Survey, Current Research, Report 08–1, p. 173–192.

McPhie, J., Doyle, M., and Allen, R.L., 1993, Volcanic textures: A guide to the interpretation of textures in volcanic rocks. Hobart, Australia, Centre for Ore Deposit and Exploration Studies, University of Tasmania, 198 p.

Morris, G. A., Larson, P. B., and Hooper, P. R., 2000, 'Subduction style' magmatism in a non-subduction setting: the Colville Igneous Complex, NE Washington State, USA: Journal of Petrology, v. 41, p. 43–67.

Nelson, J., 1997, The quiet counter-revolution: Structural control of syngenetic deposits. Geoscience Canada, v. 24, no. 2, p. 91–98.

O'Brien, B.H., 1991, Geological development of the Exploits and Notre Dame subzones in the New Bay area (parts of NTS 2E/6 and 2E/11), map area, Notre Dame Bay, Newfoundland. Newfoundland Department of Mines and Energy, Geological Survey Division, Current Research, Report 91–1, p. 155–166.

973 O'Brien, B., Swinden, H.S., Dunning, G.R., Williams, S.H., and O'Brien, F.H.C., 1997,
974 A peri-Gondwanan arc-back arc complex in Iapetus; Early-Mid Ordovician
975 evolution of the Exploits Group, Newfoundland. American Journal of Science, v.
976 297, no. 2, p. 220–272.
977 Ohmoto, H., 1996, Formation of volcanogenic massive sulphide deposits: The Kuroko
978 perspective. Ore Geology Reviews, v. 10, p. 135–177.
979 Pearce, J.A., 2008, Geochemical fingerprinting of oceanic basalts with application to
980 ophiolite classification and the search for Archean oceanic crust. Lithos, v. 100, p.
981 14–48.
982 Pearce, J.A., 1996, A user's guide to basalt discrimination diagrams, *in* Wyman, D.A.,
983 ed., Trace element geochemistry of volcanic rocks: Applications for massive
984 sulfide exploration: Geological Association of Canada, Short Course Notes, v. 12,
985 p. 79–113.
986 Pearce, J.A., and Peate, D.W., 1995, Tectonic implications of the composition of volcanic
987 arc magmas. Annual Reviews in Earth and Planetary Science, v. 23, p. 251–285.
988 Pearce, J.A., Harris, N.B.W., and Tindle, A.G., 1984, Trace element discrimination
989 diagrams for the tectonic interpretation of granitic rocks: Journal of Petrology, v.
990 25, p. 956–983.
991 Piercey, S.J., 2011, The setting, style and role of magmatism in the formation of
992 volcanogenic massive sulphide deposits. Mineralium Deposita, v. 46, p. 449–471.
993 Piercey, S.J., 2010, An overview of petrochemistry in the regional exploration for
994 volcanogenic massive sulphide (VMS) deposits. Geochemistry: Exploration,
995 Environment, Analysis, v. 10, p. 1–18.

996 Piercey, S.J., 2009, Lithogeochemistry of volcanic rocks associated with volcanogenic
997 massive sulphide deposits and applications to exploration. *In* Cousens B. and
998 Piercey, S.J. (eds.), Submarine Volcanism and Mineralization: Modern through
999 Ancient, Geological Association of Canada, Short Course 29-30 May 2008, Quebec
1000 City, Canada, p. 15–40.
1001 Piercey, S.J., Squires, G.C., and Brace, T. D., 2014, Lithostratisgraphic, hydrothermal
1002 and tectonic setting of the Boundary volcanogenic massive sulphide deposit,
1003 Newfoundland Appalachians, Canada: Formation by subseafloor replacement in a
1004 Cambrian rifted arc. Economic Geology, v. 109, p. 661–687.
1005 Piercey, S.J., Murphy, D.C., Mortensen, J.K., Creaser, R.A., 2004, Mid-paleozoic
1006 initiation of the northern cordilleran marginal back-arc basin: geological,
1007 geochemical and neodymium isotopic evidence from the oldest mafic magmatic
1008 rocks in Yukon-Tanana terrane, Finlayson Lake district, southeast Yukon, Canada.
1009 GSA Bulletin, v. 116, p.1087–1106.
1010 Pollock, J., 2004, Geology and paleotectonic history of the Tally Pond Group, Dunnage
1011 zone, Newfoundland Appalachians: An integrated geochemical, geochronological,
1012 metallogenic and isotopic study of a Cambrian island arc along the Peri-
1013 Gondwanan margin of Iapetus. Unpublished M.Sc. thesis, St. John's,
1014 Newfoundland, Memorial University of Newfoundland, 420 p.
1015 Rogers, N., and van Staal, C. R., 2002, Toward a Victorial Lake supergroup: A
1016 provisional stratigraphic revision of the Red Indian to Victoria Lakes area, central
1017 Newfoundland: Current Research – Newfoundland, Geological Survey Branch,
1018 Report 02–1, p. 185–195.

1019 Rogers, N., van Staal, C. R., McNicoll, V., Pollock, J., Zagorevski, A., and Whalen, J.,
1020 2006, Neoproterozoic and Cambrian arc magmatism along the eastern margin of
1021 the Victorial Lake supergroup: A remnant of Ganderian basement in central
1022 Newfoundland? Precambrian Research, v. 147, p. 320–341.
1023 Ross, P.-S., and Bedard, J.H., 2009, Magmatic affinity of modern and ancient subalkaline
1024 volcanic rocks determined from trace-element discriminant diagrams. Canadian
1025 Journal of Earth Sciences, v. 46, p. 823–839.
1026 Rudnick, R.L., Fountain, D.M., 1995. Nature and composition of the continental crust - a
1027 lower crustal perspective. Reviews of Geophysics, v. 33, p. 267–309.
1028 Ruks, T.W., Piercey, S.J., Ryan, J.J., Villeneuve, M.E., and Creaser, R.A., 2006, Mid- to
1029 late Paleozoic K-feldspar augen granitoids of the Yukon-Tanana terrane, Yukon,
1030 Canada: Implications for crustal growth and tectonic evolution of the northern
1031 Cordillera. Geological Society of America Bulletin, v. 118, p. 1212–1231.
1032 Shervais, J.W., 1982, Ti-V plots and the petrogenesis of modern and ophiolitic lavas.
1033 Earth and Planetary Science Letters, v. 59, p. 101–118.
1034 Spitz, G., and Darling, R. 1978, Major and minor element lithogeochemical anomalies
1035 surrounding the Louvem copper deposit, Val d'Or, Quebec. Canadian Journal of
1036 Earth Sciences, v. 15, p. 1161–1169, doi:10.1139/e78-122.
1037 Squires, G.C., and Hinchey, J.G., 2006, Geology of the Tally Pond volcanic belt and
1038 adjacent areas (parts of NTS 12A/09 & 12A/10). Government of Newfoundland
1039 and Labrador, Department of Natural Resources, Geological Survey, Map 2006-01,
1040 Open File 012A/1202.

1041 Squires, G.C., and Moore, P.J., 2004, Volcanogenic massive sulphide environments of
1042 the Tally Pond Volcanics and adjacent area: Geological, lithogeochemical and
1043 geochronological results. Newfoundland Department of Mines and Energy,
1044 Geological Survey, Current Research, Report 04–1, p. 63–91.
1045 Squires, G.C., Brace, T.D., and Hussey, A.M., 2001, Newfoundland's polymetallic Duck
1046 Pond deposit: Earliest Iapetan VMS mineralization formed within a sub-seafloor,
1047 carbonate-rich alteration system. In Evans, D.T.W., and Kerr, A. (eds.), Geology
1048 and mineral deposits of the northern Dunnage zone, Newfoundland Appalachians.
1049 Geological Association of Canada/Mineralogical Association of Canada, Field Trip
1050 Guide A2, p. 167–187.
1051 Squires, G.C., MacKenzie, A.C., and MacInnis, D., 1991, Geology and genesis of the
1052 Duck Pond volcanogenic massive sulphide deposit *In:* Swinden, H.S., Evans,
1053 D.T.W., and Kean, B.F. (eds.), Metallogenic framework of base and precious metal
1054 deposits, central and western Newfoundland. Geological Survey of Canada, Open
1055 File 2156, p. 56–64.
1056 Sun, S.-s., and McDonough, W.F., 1989. Chemical and isotopic systematics of oceanic
1057 basalts: implications for mantle composition and processes. Geological Society of
1058 London, Special Publication 42, p. 313–345.
1059 Swinden, H.S., 1991, Paleotectonic settings of volcanogenic massive sulphide deposits in
1060 the Dunnage Zone, Newfoundland Appalachians. Canada Institute of Mining and
1061 Metallurgy Bulletin, v. 84, p. 59–89.
1062 Swinden, H.S., Jenner, G.A., Kean, B.F.m and Evans, D.T.W., 1989, Volcanic rock
1063 geochemistry as a guide for massive sulphide exploration in central newfoundland.

Government of Newfoundland and Labrador, Department of Mines and Energy, Mineral Development Division (St. John's, 1985), Report of Activities 89–1, p. 201–209.

Swinden, H.S. 1996, The application of volcanic geochemistry in the metallogeny of volcanic-hosted sulphide deposits in central Newfoundland. *In* Wyman, D.A. (ed.), Trace element geochemistry of volcanic rocks: Applications for massive sulfide exploration. Geological Association of Canada, Short Course Notes, v. 12, p. 329–358.

Tatsumi, Y., and Eggins, S., 1995, Subduction Zone Magmatism. Blackwell, Cambridge.

Thurlow, J. G., 1996, Geology of a newly discovered cluster of blind massive-sulphide deposits, Pilley's Island, central Newfoundland. *In* Pereira, C. P. G., and Walsh, D. G. (eds.), Current Research Report, Report: 96–1: St. John's, NL, Geological Survey of Newfoundland and Labrador, p. 181–189.

van Staal, C.R., 1994, The Brunswick subduction complex in the Canadian Appalachians: record of the Late Ordovician to Late Silurian collision between Laurentia and the Gander margin of Avalon. Tectonics, v. 13, p. 946–962.

van Staal, C.R., 2007, Pre-Carboniferous metallogeny of the Canadian Appalachians. *In* Goodfellow, W.D. (ed.), Mineral Deposits of Canada: A Synthesis of Major Deposit Types, District Metallogeny, the Evolution of Geological Provinces, and Exploration Methods. Mineral Deposits Division, Geological Association of Canada, Special Publication 5, p. 793–818.

van Staal, C.R. and Barr, S.M., 2012, Lithospheric architecture and tectonic evolution of the Canadian Appalachians and associated Atlantic margin. Chapter 2 *in*

1087 Percival, J.A., Cook, F.A., and Clowes, R.M. (eds.), Tectonic Styles in Canada: the
1088 LITHOPROBE Perspective. Geological Association of Canada, Special Paper 49, p. 41–
1089 96.
1090 van Staal, C.R., and Colman-Sadd, S.P., 1997, The central Mobile Belt of the Northern
1091 Appalachians. Oxford Monographs on Geology and Geophysics, v. 35, p. 747–760.
1092 Vivallo, W, and Claesson, L.-Å., 1987, Intra-arc rifting and massive sulphide
1093 mineralization in an early Proterozoic volcanic arc, Skellefte district, northern
1094 Sweden. *In* Pharaoh, T.C., Beckinsale, R.D. and Rickard, D. (eds), Geochemistry
1095 and Mineralization of Proterozoic Volcanic Suites, Geological Society Special
1096 Publication No. 33, pp. 69–79.
1097 White, J.D.L., and Houghton, B.F., 2006, Primary volcaniclastic rocks. Geology, v. 34,
1098 no. 8, p. 677–680.
1099 William-Jones, A.E., Bowell, R.J., and Migdisov, A.A., 2009, Gold in solution.
1100 Elements, v. 5, p. 281–287.
1101 Williams, H., 1979, Appalachian Orogen in Canada. Canadian Journal of Earth Sciences,
1102 v. 21, p. 887–901.
1103 Williams, H., Colman-Sadd, S.P., and Swinden, H.S., 1988, Tectonostratigraphic
1104 subdivisions of central Newfoundland. In Current Research, Part B. Geological
1105 Survey of Canada, Paper 88–1B, pp. 91–98.
1106 Winchester, J.A., and Floyd, P.A., 1977, Geochemical discrimination of different magma
1107 series and their differentiation products using immobile elements. Chemical
1108 Geology, v. 20, p. 325–343.

1109 Wright, I.C., Parson, L.M., and Gamble, J.A., 1996, Evolution and interaction of
1110 migrating cross-arc volcanism and backarc rifting: An example from the southern
1111 Havre Trough (35°20'-37°S). Journal of Geophysical Research, v. 101, no. B10, p.
1112 22,071–22,086.
1113 Zagorevski, A., van Stall, C.R., Rogers, N., McNicholl, V., Dunning, G.R. and Pollock,
1114 J.C., 2010, Middle Cambrian to Ordovician are-backarc development on the
1115 leading edge of Ganderia, Newfoundland Appalachians. In From Rodinia to
1116 Pangea: The Lithotectonic Record of the Appalachian Region. Edited by R.P.
1117 Tollo, M.J. Batholomew, J.P. Hibbard, and P.M. Karabinos. Geological Society of
1118 America, Memoir 206, p. 367–396.
1119 Zagorevski, A., van Staal, C.R., McNicoll, V., Rogers, N., and Valverde- Vaquero, P.,
1120 2008, Tectonic architecture of an arc-arc collision zone, Newfoundland
1121 Appalachians. *In* Draut, A., Clift, P.D., and Scholl, D.W. (eds.), Formation and
1122 Applications of the Sedimentary Record in Arc Collision Zones. Geological Society
1123 of America, Special Paper 436, p. 309–334.
1124 Zagorevski, A., van Staal, C.R., McNicoll, V.J., and Rogers, N., 2007b, Upper Cambrian
1125 to Upper Ordovician peri-Gondwanan island arc activity in the Victorial Lake
1126 supergroup, central Newfoundland: Tectonic development of the northern
1127 Ganderian margin. American Journal of Science, v. 307, p. 339–370.
1128 Zagorevski, A., van Staal, C.R., and McNicoll, V.J., 2007a, Distinct Taconic, Salinic, and
1129 Acadian deformation along the Iapetus suture zone, Newfoundland Appalachians.
1130 Canadian Journal of Earth Sciences, v. 44, p. 1567–1585.

1131 Zagorevski, A., Rogers, N., McNicoll, V., Lissenberg, C.J., van Stall, C.R., and
1132 Valverde-Vaquero, P., 2006, Lower to Middle Ordovician evolution of peri-
1133 Laurentian arc to back-arc complexes in the Iapetus: Constrains from the
1134 Annieopsquotch accretionary tract, central Newfoundland. Geological Society of
1135 America Bulletin, v. 118, no. 3/4, p. 324–342.
1136

## Figures

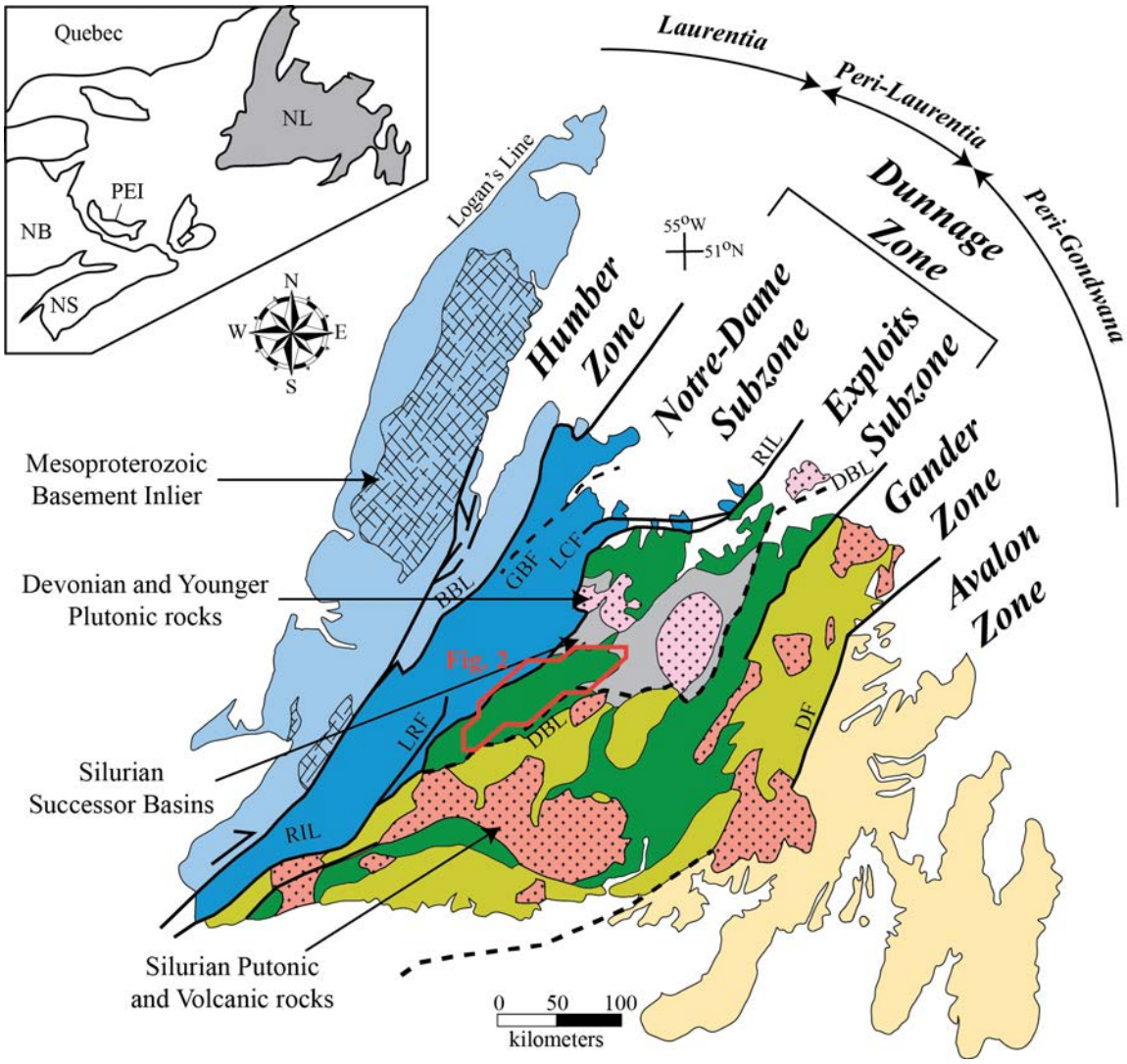


Figure 1. Simplified geological map of the Newfoundland with tectonostratigraphic zones (modified from van Staal 2007, and van Staal and Barr 2012). Abbreviations are as follow: BBL: Baie Verte Brompton Line, DBL: Dog Bay Line, DF: Dover Fault, GBF: Green Bay fault, LCF: Lobster Cove fault, LRF: Lloyds River fault, and RIL: Red Indian Line.

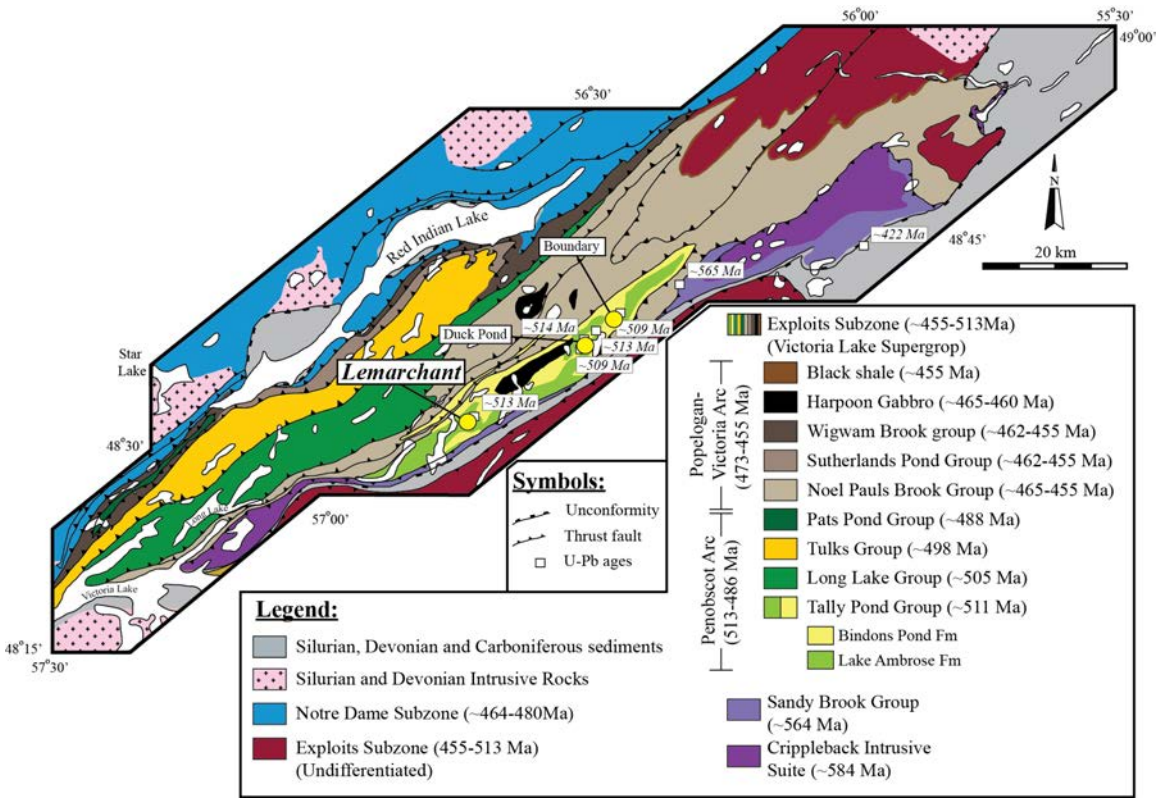


1144

1145 Figure 2: Geologic setting of the Victoria Lake supergroup, as well as the VMS deposit

1146 hosted within the Tally Pond group. Diagram modified from McNicoll et al. (2010) and

1147 Piercey et al. (2014).

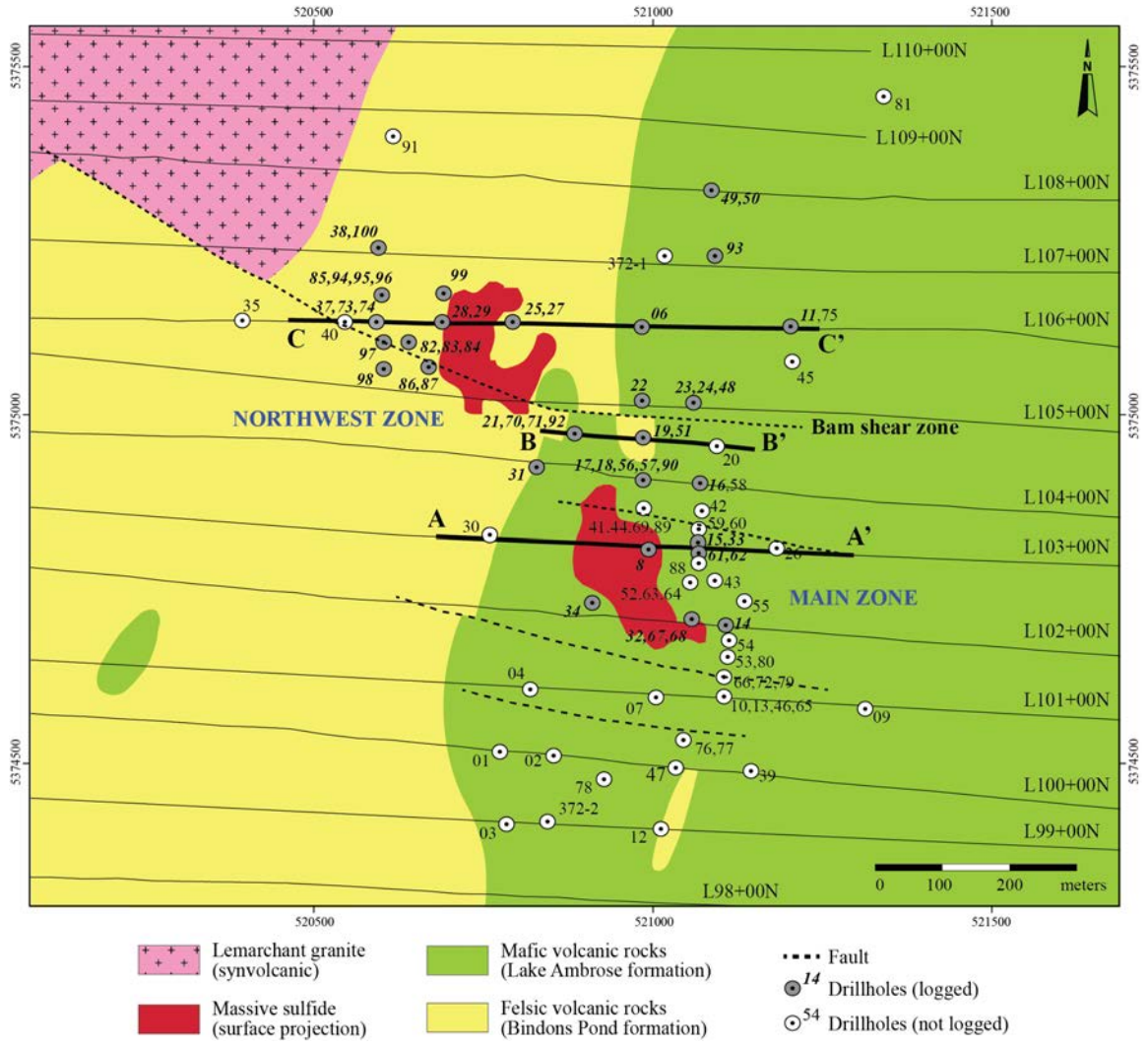


1148

1149 Figure 3: Geological map of the Lemarchant area and projected surface location of the

1150 Main and Northwest mineralised zones. Also shown are the cross-section lines (A-A', B-

1151 B', and C-C') described in figure 5. Map modified from Fraser et al. 2012.

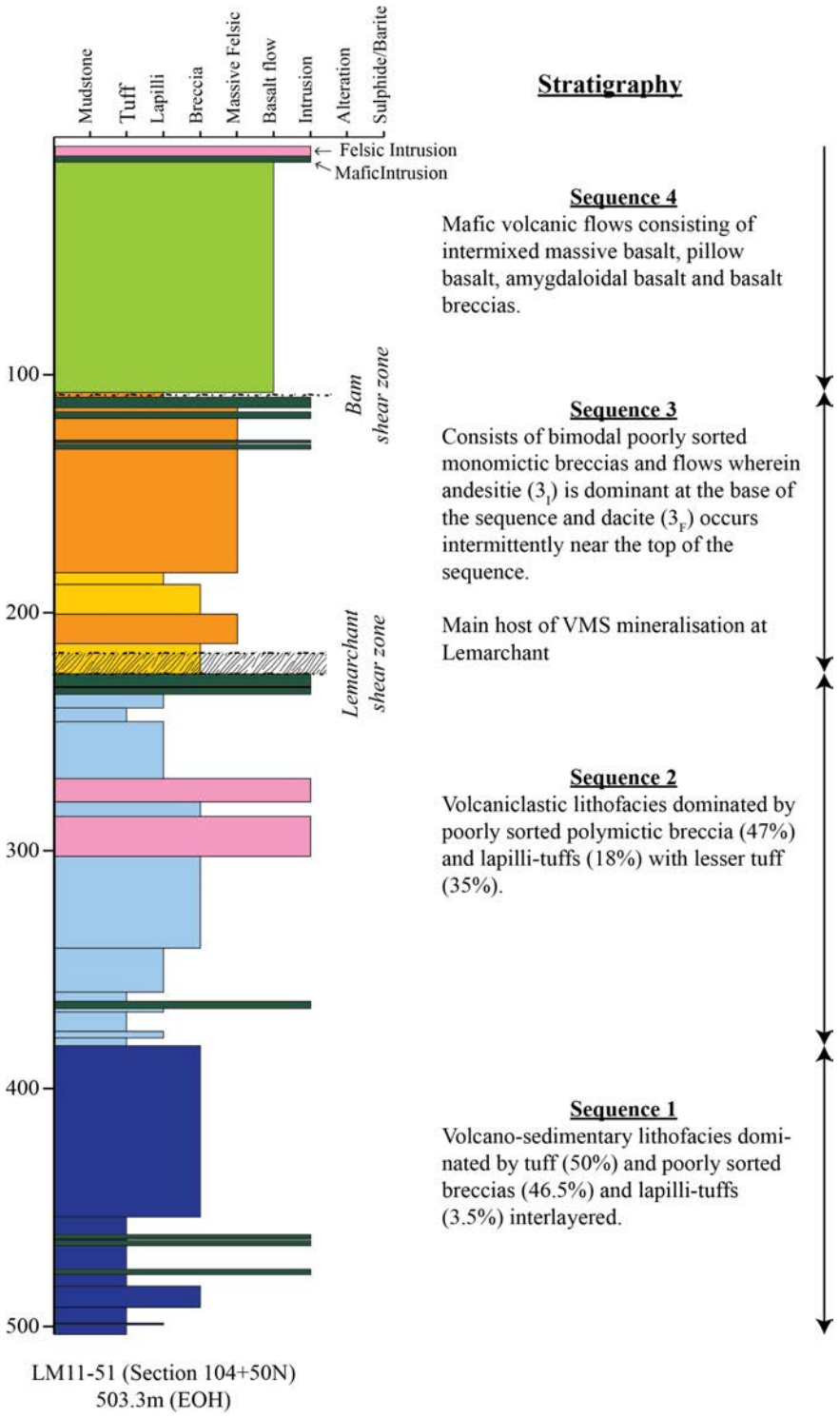


Figure 4: Lithostratigraphic sequence from drill core LM11-51 (section 104+50N) representative of the Lemarchant area. Also shown is the summary of the key features of each sequence.

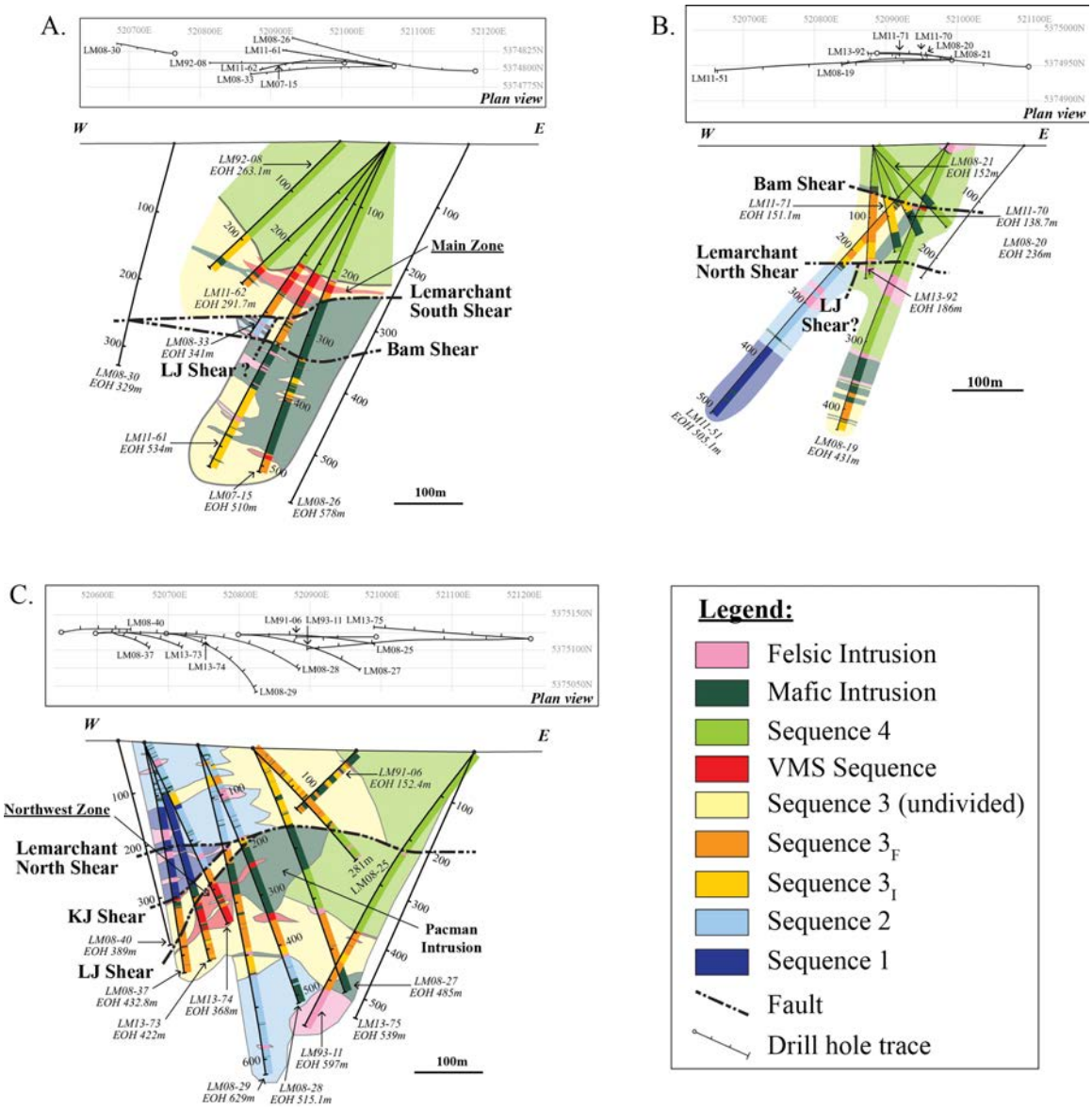


Figure 5: Cross-section along (A) the southern portion (section 103+00N; Main Zone), (B) the central portion (section 104+50N, and (C) the northern portion (106+00N; Northern Zone) of the Lemarchant area.

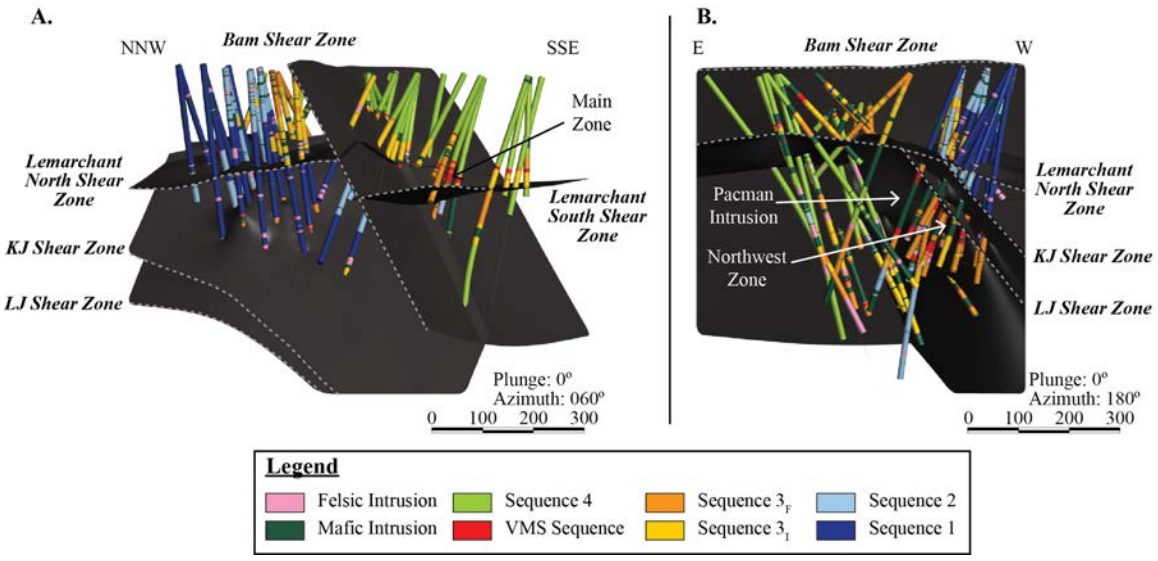


1160

1161 Figure 6: Three-dimension representation of the lithostratigraphic sequences logged

1162 during this study. Also shown are the structural elements present in the Lemarchant area

1163 and the location of the Main and Northwest mineralised zones. (A) Looking ENE (060º)

1164 and (B) looking south (180º).

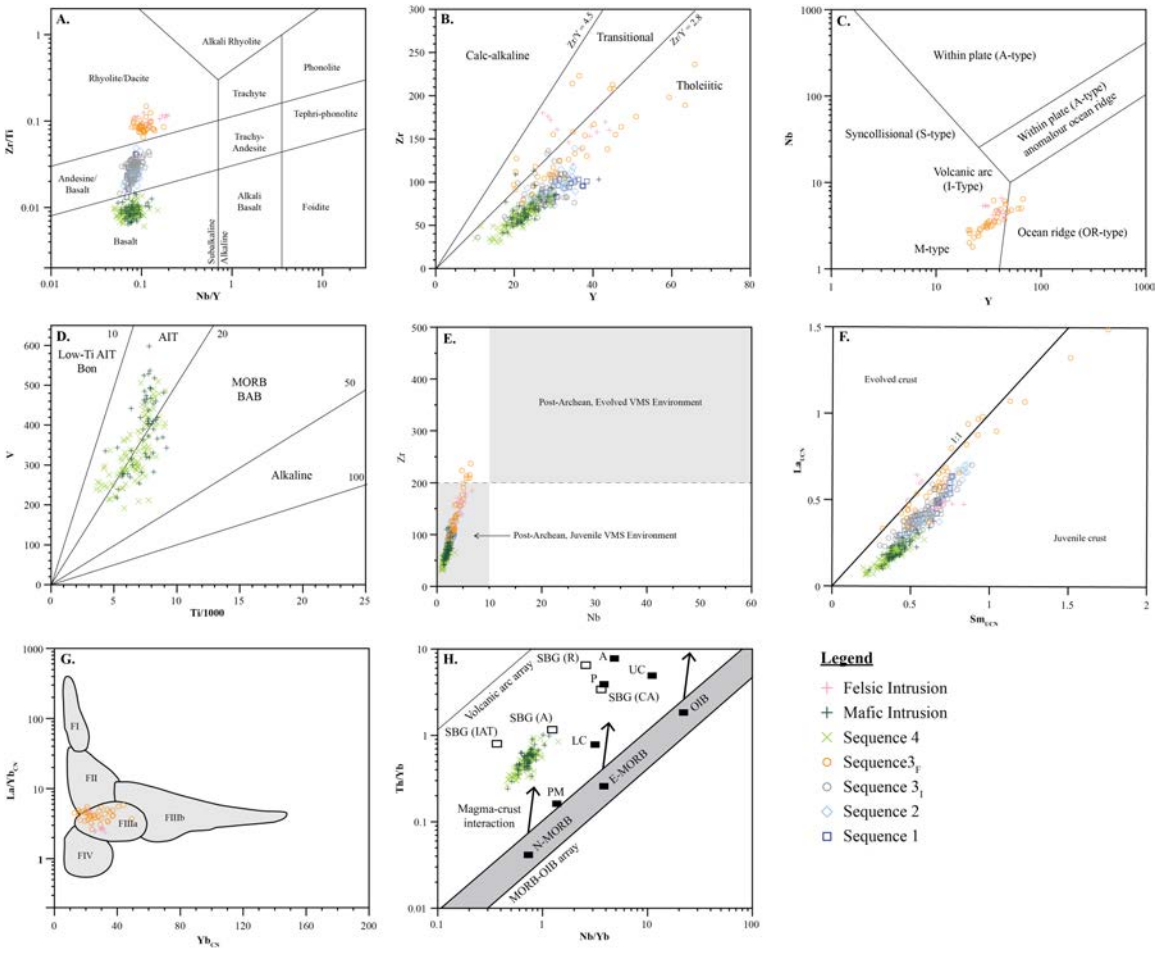


1165

1166 Figure 7: Immobile element discrimination diagrams for the volcanic rocks from the
1167 Lemarchant area. (A) Zr/TiO2-Nb/Y (Winchester and Floyd 1977) with modified field
1168 boundaries of Pearce (1996). (B) Zr-Y discriminating magma affinity with fields of Ross
1169 and Bedard (2009). (C) Nb-Y with field boundaries of Pearce et al. (1984) for felsic
1170 rocks. (D) V-Ti/1000 diagram with field boundaries of Shervais (1982) for mafic rocks.
1171 (E) Zr-Nb diagram of Piercey (2009) discriminating juvenile environments from evolved
1172 environments. (F) Upper-crust normalised (UCN) La-Sm diagram (normalisation values
1173 from McLennan, 2001). (G) $La/Yb_{CN}$-$Yb_{CN}$ FI-FIV rhyolite discrimination diagram
1174 (chondrite normalised values (CN) from McDonough and Sun, 1995; diagrams from
1175 Lesher et al., 1986; and Hart et al., 2004). (H) Th/Yb-Nb/Yb diagram of Pearce (2008)

1176 for mafic volcanic rocks. Also shown in (H) are the average composition of the lower
1177 crust (LC), upper crust (UC), felsic Phanerozoic (P) and Archean (A) crust from Rudnick
1178 and Fountain (1995), and average composition of the Sandy Brook Group (SGB) island
1179 arc tholeiite (IAT), andesite (A), and rhyolite (R) from Rogers et al. (2006).

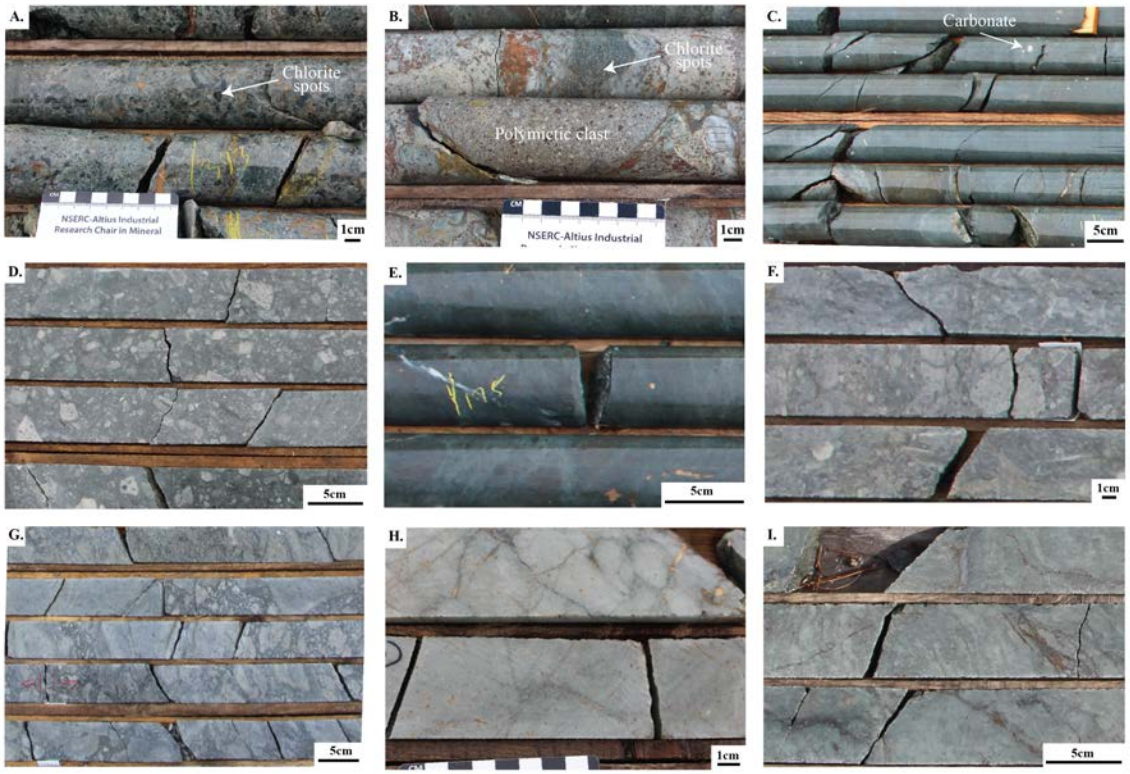


1180

1181 Figure 8: Intermediate and felsic volcanic rocks the Lemarchant area. (A) Polymictic
1182 breccias with characteristic chlorite spots from sequence 1; sample LM11-51_393m. (B)
1183 Polymictic breccia with polymictic clasts from sequence 1; sample LM08-37_266m. (C)
1184 Felsic tuff from sequence 1;sample LM08-37_145.5m. (D) Polymictic breccias from
1185 sequence 2; sample LM13-82_041m. (E) Felsic tuff from sequence 2; sample LM14-
1186 98_175.0m. (F) Intermediate monomictic breccia from sequence $3_I$; sample LM11-
1187 71_94m. (G) Felsic monomictic breccia from sequence $3_F$; sample LM13-86_101m. (H)
1188 Intermediate jigsaw-fit flow from sequence $3_I$; sample LM11-51_150.0m. (I) Felsic flow-
1189 banded flow from sequence $3_F$; sample LM08-37_326.3m. All drill core samples are from
1190 NQ core (diameter = 47.6 mm).

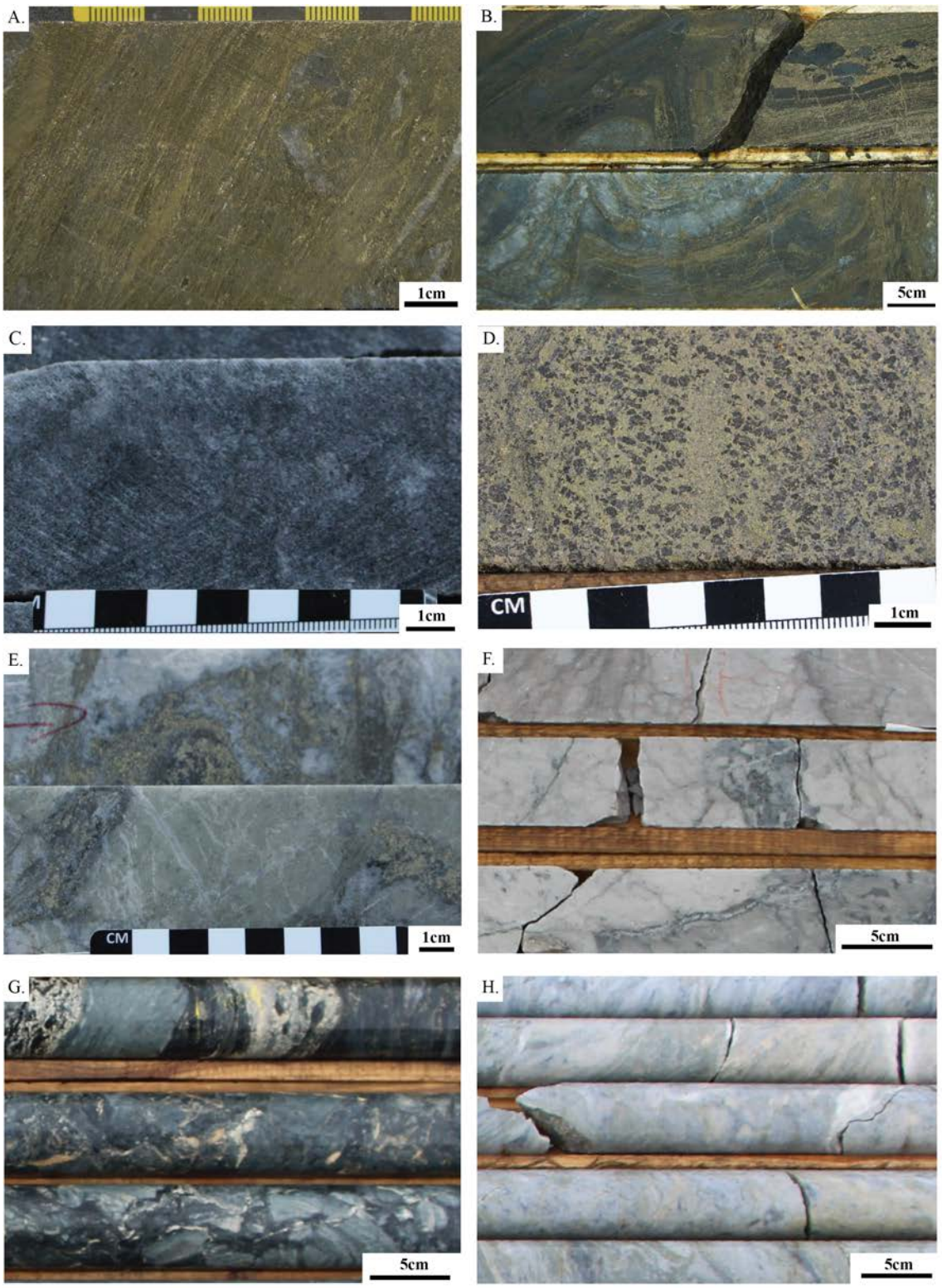


1191

1192 Figure 9: Rocks associated with the Lemarchant VMS system (A) Weakly sheared

1193 exhalative mudstone sample from the Main Zone; sample LM11-68_196.95m. (B) Highly

deformed and folded exhalative mudstone interlayered with tuff from the Northwest Zone; sample LM13-83_300.2m. (C) Unmineralised granular massive barite; sample LM13-73_336m. (D) Massive sulphides from the Northwest Zone consisting of chalcopyrite, sphalerite and pyrite; sample LM13-73_349.9m. (E) Semi-Massive sulphides from the Northwest Zone consisting of dissemination and veins of honey brown sphalerite and pyrite filling interstices among the jigsaw breccia fragments felsic flow. Weak chlorite, sericite and silica alteration occurs with the semi-massive sulphides; sample LM11-73_306m. (F) Silica alteration of an intermediate massive flow; sample LM13-82_336.3m. (G) Pervasive chlorite-carbonate alteration of a layered massive felsic flow; sample LM13-83_368.0m. (H) Sericite and silica altered felsic massive flow; sample LM13-87_356.3m. All drill core samples are from NQ core (diameter = 47.6 mm).

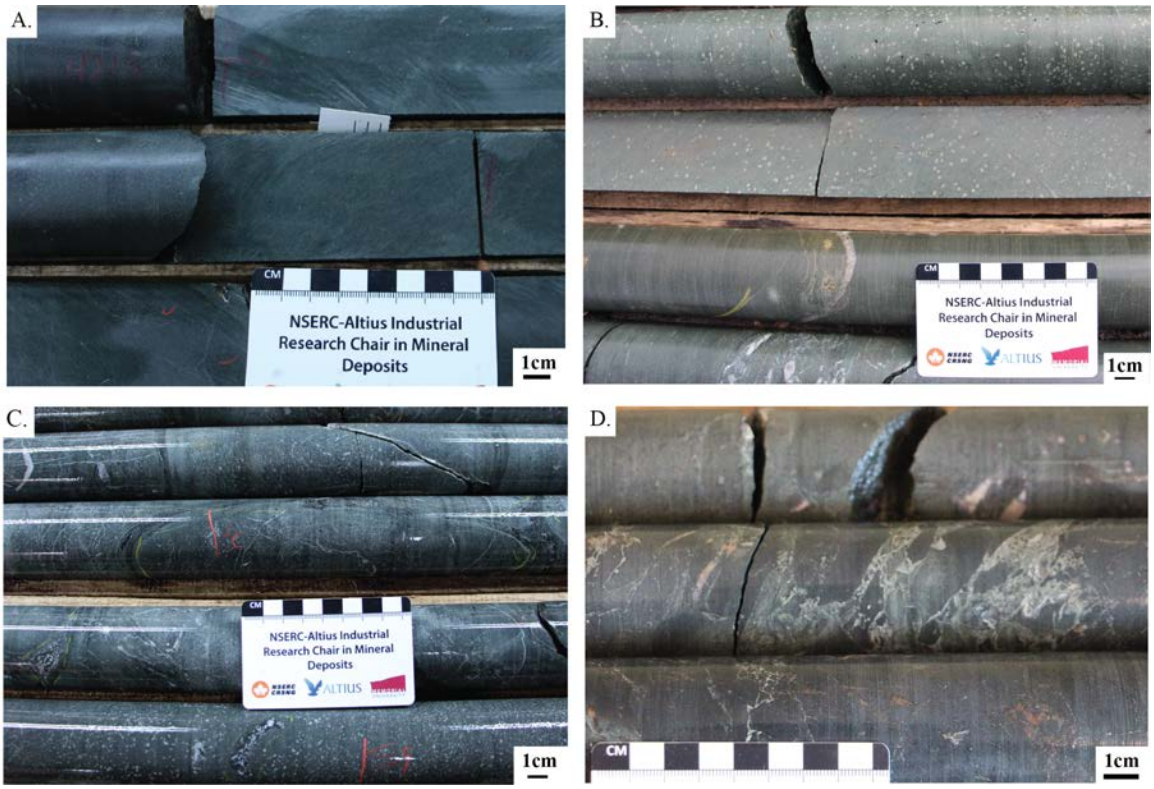


Figure 10: Mafic rocks from sequence 4. (A) Massive basalt; sample LM11-49_421.3m. (B) Amygdaloidal basalt; sample LM07-16_106m. (C) Pillow basalt; sample LM11-49_056m. (D) Basalt breccia; sample LM07-16_046.2m. All drill core samples are from NQ core (diameter = 47.6 mm).

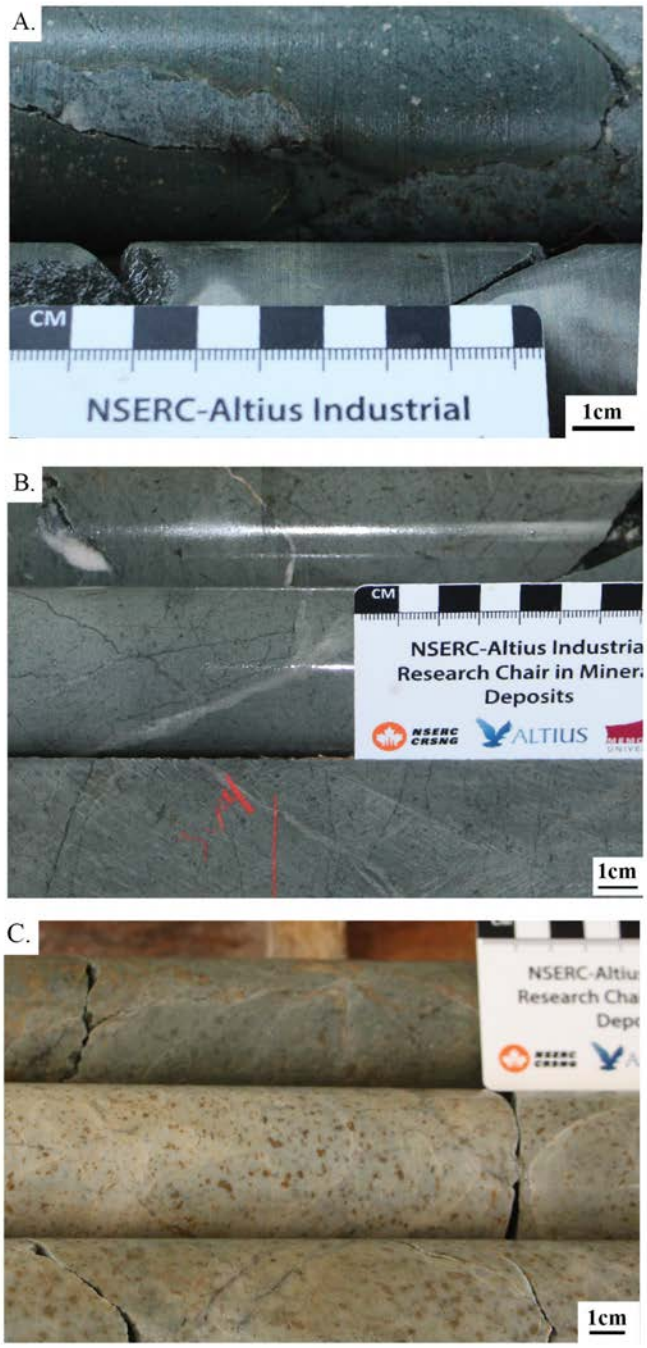


1211

1212 Figure 11: Intrusions from the Lemarchant area. (A) Mafic intrusion; sample LM08-

1213 37_108.4m. (B) Intermediate intrusion; sample LM11-49_343m. (C) Felsic intrusion;

1214 sample LM08-34_318m. All drill core samples are from NQ core (diameter = 47.6 mm).

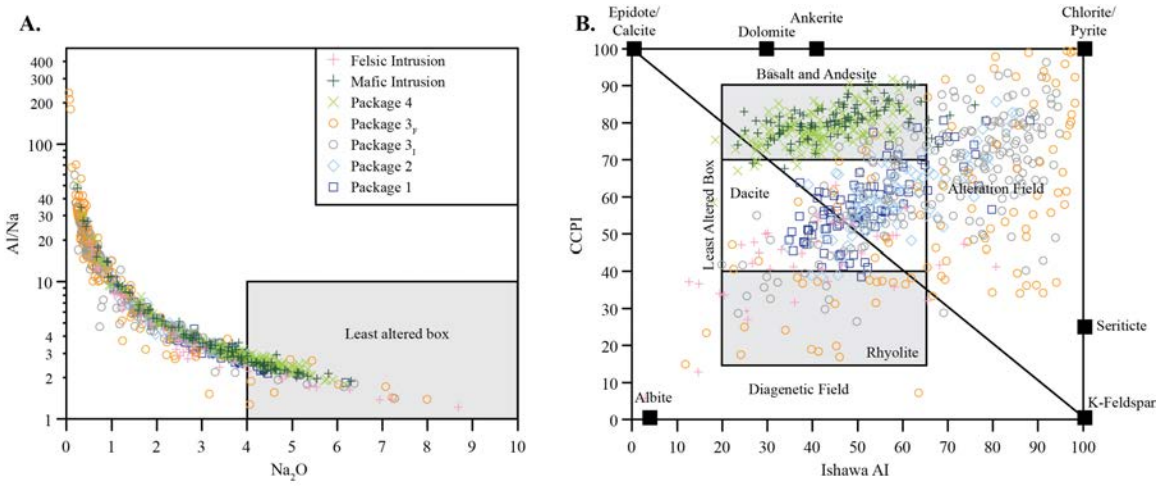


1215

1216 Figure 12: Mobile element plots for the rocks from the Lemarchant VMS deposit. (A)

1217 Spitz-Darling (Spitz and Darling 1978) index versus $Na_2O$ (diagram after Ruks et al.

1218 2006). (B) Alteration box plot with the AI index (AI; Ishikawa et al. 1976) plotted against

1219 the chlorite-carbonate-pyrite index (CCPI; Large et al. 2001).

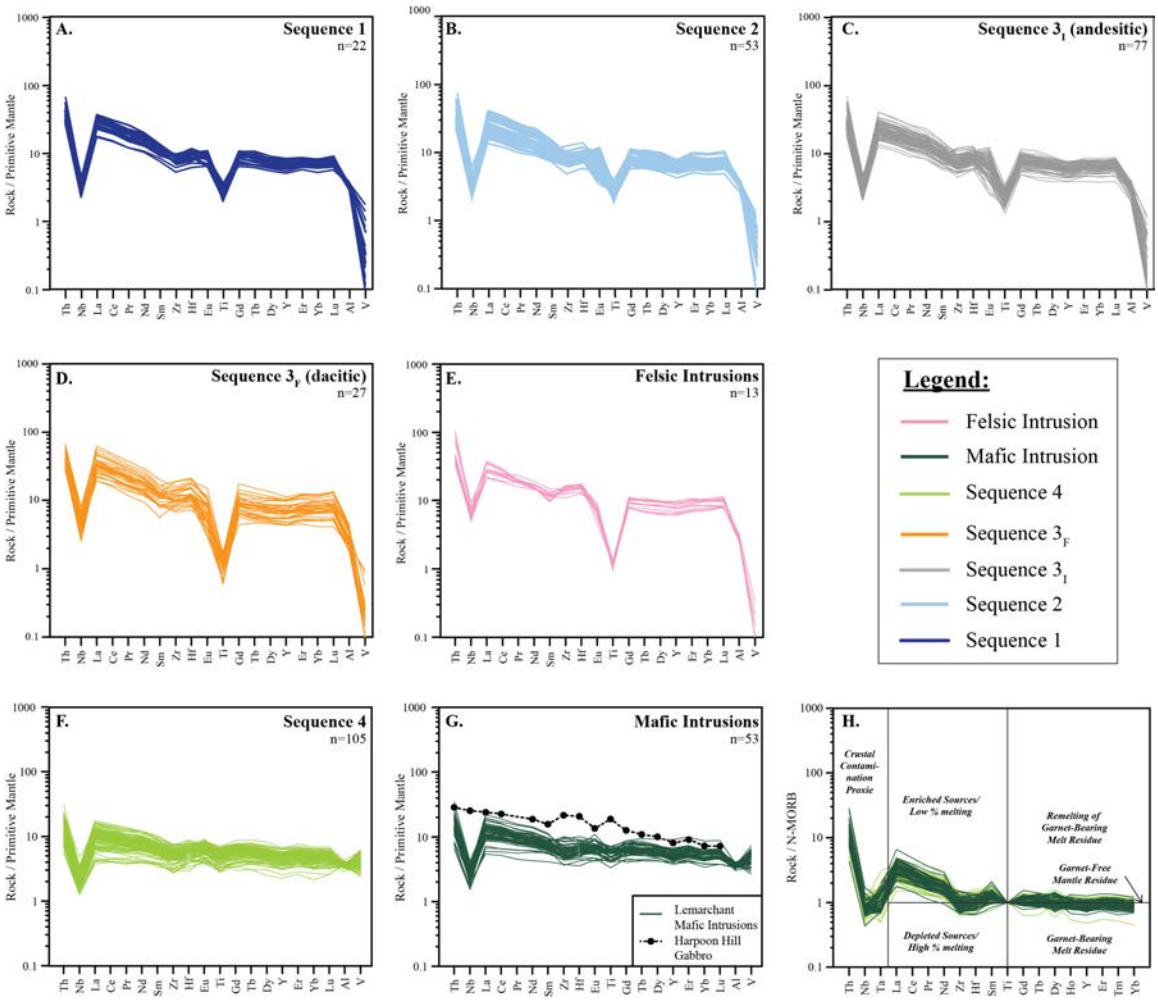


Figure 13: Primitive mantle normalised extended REE element profiles for the rocks from the Lemarchant area. (A) sequence 1, (B) sequence 2, (C) sequence $3_I$ (andesitic), (D) sequence $3_F$ (dacitic), (E) felsic intrusions, (F) sequence 4, (G) mafic intrusions, and (H) mafic volcanic rocks normalised to N-MORB, and subsequently renormalised to Ti (Ti = 1) with the tectonic fields of Pearce (2008). In all, normalisation factors are from Sun and McDonough (1989).

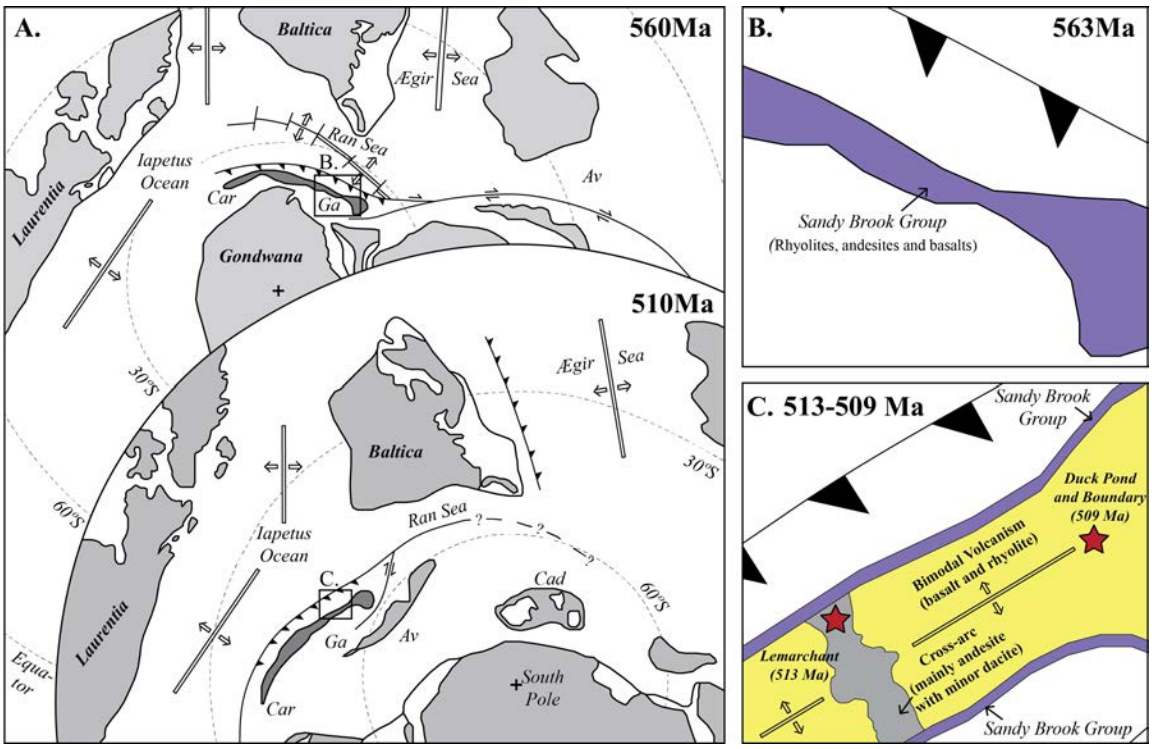


Figure 14: Neoproterozoic to middle Cambrian paleogeographic reconstructions of the distribution of the continental landmasses within the southern hemisphere (modified from Rogers et al., 2006). (A) The Lemarchant deposit likely formed in southern latitudes in a peri-Gondwanan setting along the edge of Ganderia. The location of the potential environment of the Lemarchant deposit is outlined in the black box. (B) Early stage (563 Ma). Formation of the Sandy Brook Group within a magmatic arc. (C) Syn-mineralisation stage (513-509 Ma). Rifting of the 563 Ma Sandy Brook Group magmatic arc and emplacement of the Tally Pond Group within the rifted zone. The Lemarchant deposit likely formed within a migrating cross-arc at shallow water depth (<1500 metres below sea level), which permitted the hydrothermal fluid boiling and deposition of precious metals. Abbreviations are as follow: Av: Avalonia; Cad: Cadomia; Car: Carolina Terrane; and Ga: Ganderia (darker grey shading).

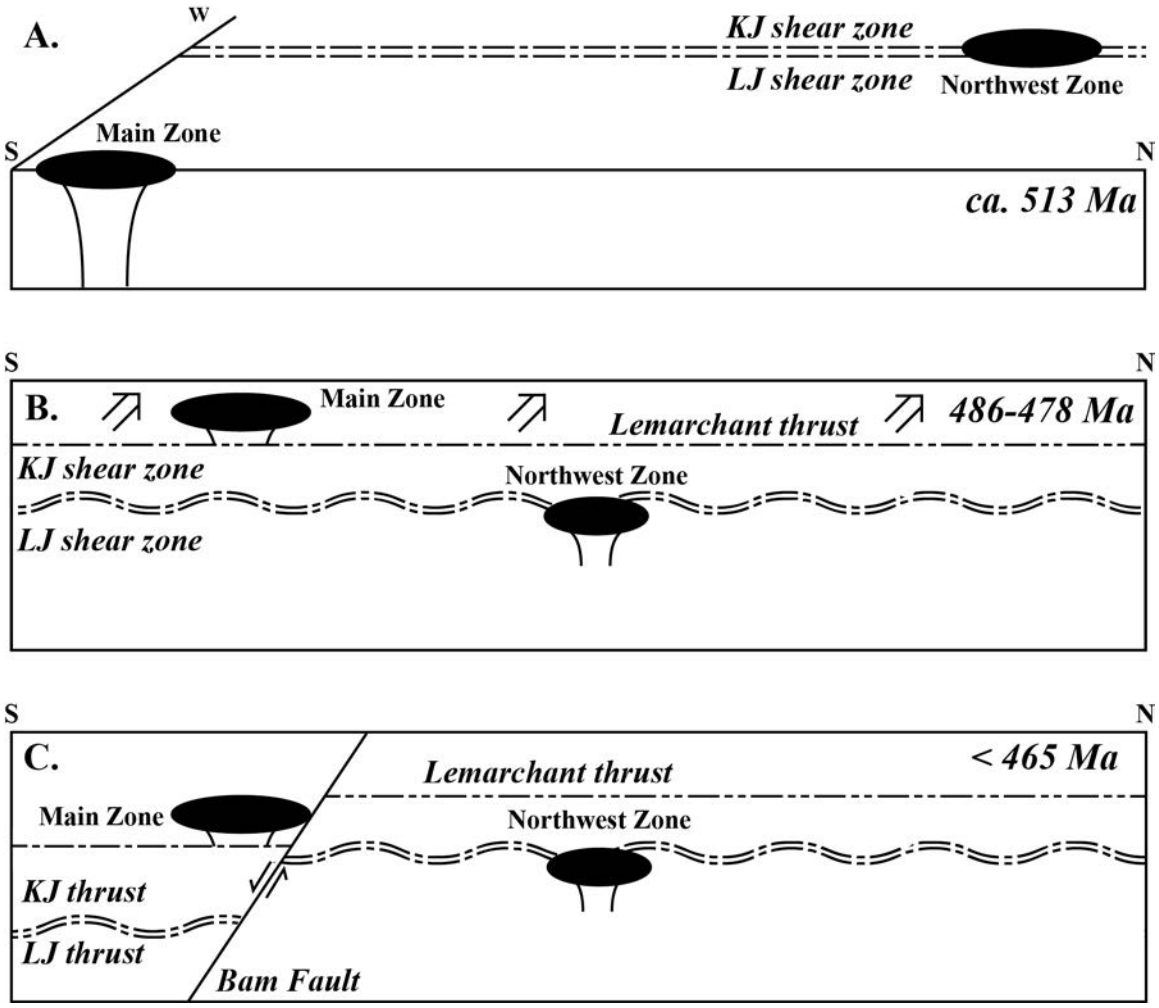


Figure 15: Geotectonic evolution of the Lemarchant area. (A) Formation stage (513-509 Ma). The Main Zone and the Northwest Zone forms on or near the seafloor. (B) Main deformation stage (485-478 Ma). The LJ and KJ syn-volcanic shear zones are deformed and the Lemarchant thrust is emplaced thrusting the Main zone on the south of the current location of the Northwest Zone. (C) Late deformation stage (< 465 Ma). Normal extension episode marked by the creation of the west striking Bam normal fault.